SAPIENZA
Università di Roma
Facoltà di Farmacia e Medicina

Ph.D. in
MORPHOGENESIS AND TISSUE ENGINEERING

XXXVIII Ciclo
(A.A. 2025/2026)

Role of Epigenetic and Metabolic Reprogramming in Normal and Neoplastic Hematopoiesis

Ph.D. Student
Alessandra Zaza

Tutor
Prof. Clara Nervi
Prof. Nelida Ines Noguera

Coordinator
Prof. Antonio Filippini

Sommario

1. SUMMARY

Acute Myeloid Leukemias (AMLs) are aggressive hematologic malignancies sustained by profound metabolic rewiring and altered redox balance. We characterized the bioenergetic profile of normal bone marrow (NBM) progenitors and AML blasts, and investigated the metabolic, antioxidant, and epigenetic vulnerabilities associated with the PLZF::RARa fusion protein, a rare variant of acute promyelocytic leukemia (APL) resistant to differentiation therapy.

Our analyses revealed that AML blasts display higher basal glycolysis, glycolytic reserve, and oxidative phosphorylation (OXPHOS) compared to normal progenitors. Elevated proton leak and spare respiratory capacity, suggest a metabolic adaptation that confers survival advantage and therapy resistance. In PLZF::RARa-positive U937-B412 cells, we observed enhanced mitochondrial respiration and reactive oxygen species (ROS) production, accompanied by NRF2 protein destabilization and reduced transcriptional activity of its antioxidant targets (HO-1, G6PDH).

At the epigenetic level, we identified the nuclear transposition of miR-223 which binds, among others, metabolism-related genes' regulating sequences, including SIRT1. In fact, in B412 cell line, PLZF::RARa expression reduced SIRT1 levels, increased acetylation of the transcription factor FOXO3a, and impaired expression of its antioxidant target genes SOD1 and Catalasi. These findings indicate that PLZF::RARa impairs cellular antioxidant capacity. These vulnerabilities can be exploited through metabolic and redox-oriented strategies. High-dose ascorbate acts as a pro-oxidant, enhancing ROS to selectively eliminate leukemia cells, while azacitidine (a DNA hypomethylating agent) and venetoclax (a BCL-2 inhibitor that compromises OXPHOS) act synergistically to target the survival of leukemia stem cells.

Targeting metabolic-epigenetic-redox pathways offers promising alternatives to conventional chemotherapy, especially in PLZF::RARa+ APL subtypes, which are resistant to therapies.

2. INTRODUCTION

Hematopoiesis is a highly intricate and precisely regulated biological process responsible for the generation of diverse blood cell linages, each performing specialized and critical functions, including oxygen transport, immune surveillance, and tissue homeostasis.

2.1 Hematopoiesis

Hematopoietic stem cells (HSCs) sustain hematopoiesis throughout life[1]. During embryonic development, HSCs undergo several rounds of cell division while preserving their exceptional capacity for self-renewal and regeneration, largely attributed to their high DNA repair activity and metabolic flexibility [2, 3]. This regenerative potential, however, decreases significantly with age. In adulthood, HSCs enter a predominantly quiescent state, characterized by reduced proliferative activity and a reliance on anaerobic metabolism. This metabolic profile is essential for preserving their stem cell properties and preventing premature exhaustion over the lifespan[4]. Human HSCs can be isolated from bone marrow, peripheral blood and umbilical cord blood. Phenotypically, they are typically CD34-positive (where CD34 function as a cell adhesion molecule) and CD38-negative or low (CD38 is a multifunctional enzyme highly expressed in differentiated leukocytes).

During hematopoietic cell differentiation, HSCs undergo lineage commitment through tightly regulated developmental pathways, governed by a complex interplay of intrinsic transcription factors and extrinsic signals such as cytokines and growth factors. These regulatory cues are provided by the bone marrow microenvironment, known as the hematopoietic niche[5, 6]. However, with aging, the hematopoietic niche undergoes structural and functional changes that, together with the accumulation of somatic mutations in HSC, compromise their self-renew capacity

and differentiation potential[7]. This age-related decline is characterized by reduced clonal diversity and capacity for lymphoid lineage commitment, and a propensity toward myeloid-biased hematopoiesis[5, 8].
Hematopoietic stem cells differentiate into pluripotent stem cells which, in turn, gives rise to two lineages: lymphoid and myeloid[9]. The lymphoid lineage includes T cells, NK cells, and B cells. The myeloid lineage includes red blood cells, megakaryocytes, macrophages, neutrophils, basophils, and eosinophils. A schematic representation of the hematopoietic maturation pathways is shown in Figure 1.

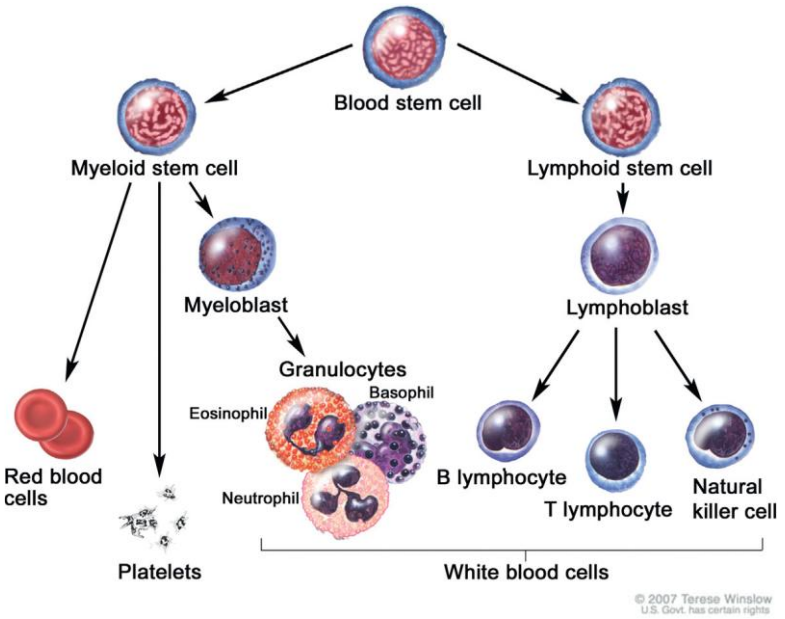

Figure 1. Normal differentiation pathways for the differentiation of various blood cells. Brody T. *Clinical Trials*. Elsevier, 2016. Chapter 18: Hematological Cancers.

Alterations affecting the lymphoid lineage can lead to the development of lymphoid neoplasms, while disruptions in the myeloid lineage are associated with the emergence of myeloid

neoplasms[10]. The myelodyplastic syndromes are a subset of myeloid neoplasms[11].
Under normal physiological conditions, undifferentiated blood stem cells, also known as blast cells, constitute up to 5% of the total cellular population within the bone marrow. They are identifiable by their relatively large size and immature nuclear morphology. The presence of blast cells in the circulation is considered abnormal and is a hallmark of hematologic malignancies, most notably acute leukemias [12].

2.2 Acute myeloid leukemia

Acute Myeloid Leukemias (AMLs) are hematologic malignancies characterized by clonal proliferation and accumulation of immature myeloid cells with impaired differentiation. AML blasts infiltrate the bone marrow, peripheral blood, and sometimes extramedullary tissues. Metabolic, genetic, and epigenetic alterations drive their uncontrolled growth and hinder normal myeloid precursor differentiation [13, 14].

The occurrence of hematological malignancies, in particular Myelodisplastic syndromes (MDSs) and AMLs, has been linked to the depletion of stem cell clone diversity: a phenomenon known as age-related clonal hematopoiesis (ARCH) occurring by age 70 in about 10% of healthy individuals[15]. Approximately 30% of AMLs cases are secondary to Myelodysplastic syndromes (MDS). MDS are a heterogeneous group of myeloid neoplasms defined by distinct genetic and clinical features characterized by peripheral cytopenias, bone marrow (BM) failure, morphologic dysplasia in one or more hematopoietic lineages, and genetic instability that eventually leads to transformation in secondary AMLs.

AMLs represent the most common acute leukemia in adults, accounting for approximately 80 percent of cases in this population[16]. Its incidence increases with age, from 1.3 per

100,000 individuals in those aged 65 years old to 12.2 per 100,000 in those aged 65 years and older. Although advances in the treatment of AML have led to significant improvements in outcomes for younger patients, prognosis in the elderly, who account for the majority of new cases, remains poor[17].

Age-related stochastic events may initially favor the expansion of ARCH clones. Subsequent mutational events, together with their proliferation under selective pressure, drive leukemic initiation and progression. As a result, a progressive accumulation of blasts occurs, initially in the bone marrow and later in the peripheral blood and other tissues.

The altered genes characterizing AMLs can be subdivided into five categories (Figure 2): Class I mutations, activators of tyrosine kinase, provide the hematopoietic progenitors with survival/proliferation advantage; Class II mutations, transcriptional factors such as NPM1, CEBPA, and TP53 as well as oncogenic fusion genes (PML::RARa), arrest the differentiation of hematopoietic cells; Class III mutations, epigenetic regulatory molecules (DNMT3A and HDACs), silence/activate the tumor suppressor genes/pro-tumor genes; Class IV mutations involve genes that alter cell adhesion and cell-cell interaction, leading to the flexible migration; Class V mutation includes genes dysregulating DNA-repair and RNA-splicing[18].

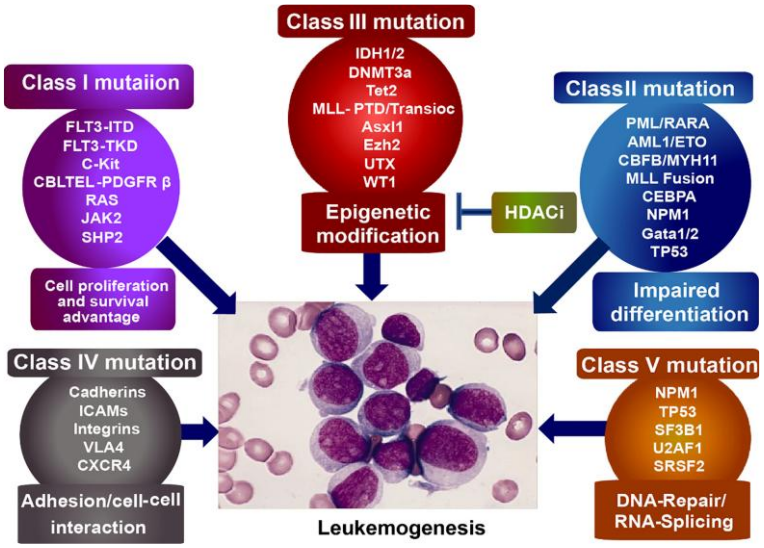

Figure 2. Classification based on mutagenic genes linked to leukemogenesis. (Readapted from Zhang et al. Frontiers in Oncology, 2021).

2.3 Classification of AML

AML subtypes were initially categorized morphologically, according to the French-American-British (FAB) system, into eight subtypes from M0 to M7 based on the leukemic cell maturation/differentiation: M0, undifferentiated myeloblastic leukemia; M1, acute myeloblastic leukemia without maturation; M2, acute myeloblastic leukemia with maturation; M3, acute promyelocytic leukemia; M4, acute myelomonocytic leukemia; M5, acute monocytic leukemia; M6, acute erythroid leukemia; M7, acute megakaryoblastic leukemia. The World Health Organization (WHO) classification, which integrates morphological, cytogenetic, and molecular features, replaced the previous. Following the FAB classification, in 1998, the World Health Organization introduced the WHO (World Health Organization) classification, which today, together with the ICC (International Consensus Classification), are the most widely used classifications in the field of diagnostics. The

latest revision of the WHO and ICC classifications dates back to 2022; the classification of haematolymphoid neoplasms of the WHO classification, now in its fifth edition, is referred to as "WHO-HAEM5"[19, 20]. The WHO-HAEM5 classification divides LAM into two main families: LAM with defined genetic abnormalities and LAM defined by differentiation (Table 1).

Acute myeloid leukaemia with defining genetic abnormalities
Acute promyelocytic leukaemia with *PML::RARA* fusion
Acute myeloid leukaemia with *RUNX1::RUNX1T1* fusion
Acute myeloid leukaemia with *CBFB::MYH11* fusion
Acute myeloid leukaemia with *DEK::NUP214* fusion
Acute myeloid leukaemia with *RBM15::MRTFA* fusion
Acute myeloid leukaemia with *BCR::ABL1* fusion
Acute myeloid leukaemia with *KMT2A* rearrangement
Acute myeloid leukaemia with *MECOM* rearrangement
Acute myeloid leukaemia with *NUP98* rearrangement
Acute myeloid leukaemia with *NPM1* mutation
Acute myeloid leukaemia with *CEBPA* mutation
Acute myeloid leukaemia, myelodysplasia-related
Acute myeloid leukaemia with other defined genetic alterations
Acute myeloid leukaemia, defined by differentiation
Acute myeloid leukaemia with minimal differentiation
Acute myeloid leukaemia without maturation
Acute myeloid leukaemia with maturation
Acute basophilic leukaemia
Acute myelomonocytic leukaemia
Acute monocytic leukaemia
Acute erythroid leukaemia
Acute megakaryoblastic leukaemia

Table 1. WHO-HAEM5 classification for LAM [21]

Most AML with defined genetic abnormalities can be diagnosed with a blast percentage <20%, with the exception of AML with BCR/ABL1 fusion and AML with CEBPA mutation. Compared to the previous revision, "AML with myelodysplasia-related changes

is referred to as AML-MRC [21]. The 2022 ICC classification, compared to the last revision in 2016, eliminates the following categories: therapy-related AML, AML with myelodysplasia-related disorders (MDS and MDS/MPN), and AML related to germline genetic disorders [22].

The main categories of ICC (Fig. 3) are therefore:
- AML with recurrent genetic alterations.
- AML with mutated TP53.
- AML with myelodysplasia-related gene mutations.
- AML with myelodysplasia-related cytogenetic abnormalities.
- AML not otherwise specified (NOS)

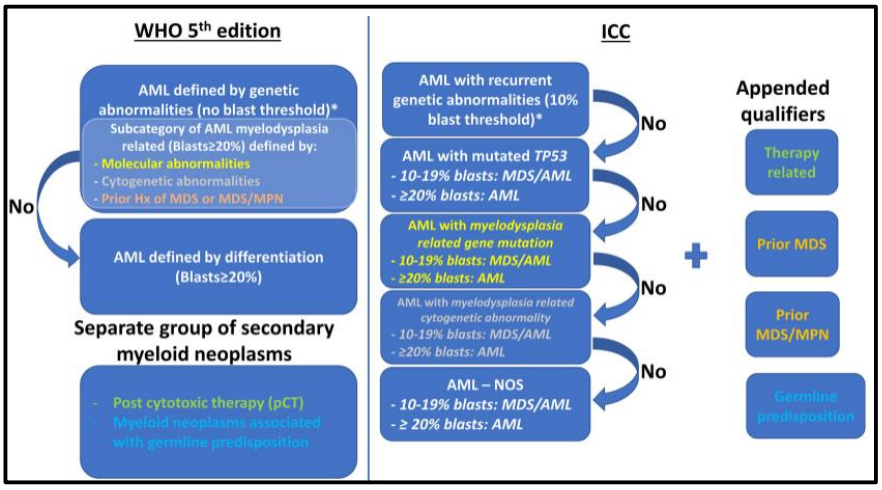

Figure 3. WHO-HAEM5 classification vs. ICC [19]

2.4 PLZF::RARa-associated APL

Acute promyelocytic leukemia (APL) is a distinct subtype of AML characterized, in approximately 95% of cases, by the presence of the PML::RARa fusion gene, resulting from the traslocation between the promyelocytic leukemia (PML) gene on chromosome 15 and the retinoic acid receptor α (RARa) gene on chromosome 17 [t(15;17)

(q24;q21)][23]. Other, less common rearrangements and fusion genes have also been reported to cause an APL-like phenotype. Among them, PLZF::RARa (ZBTB16-RARα) accounts for about 2% of all APL cases[24]. PLZF::RARa fusion gene, results from a chromosomal translocation involving PLZF (promyelocytic leukemia zinc finger; known as ZBTB16) on chromosome 11 and the RARa gene on chromosome 17, [t(11;17) (q23;q21)].

The phenotype of these APL blasts may include either regular or irregular nuclei, abundant cytoplasm containing coarse or fine granules, and the presence of Auer rods[25, 26].

The N-terminal portion of PLZF comprises: i) the POZ (Pox virus and zinc finger) or BTB (Broad Complex, tramtrack, Bric-à-Brac) domain, which is essential for self-association, DNA looping, repression of gene transcription, and histone deacetylation; ii) the RD2 domain, which contribute to the transcriptional activation of several genes.

The C-terminal portion contains nine C_2H_2-type zinc fingers that facilitate the interaction of PLZF with its target DNA sequences. [27]. The PLZF::RARa fusion protein functions predominantly as a transcriptional repressor by recruiting histone deacetylases (HDACs) and polycomb repressive complexes (PRCs), thereby enforcing epigenetic silencing[28, 29].

Pharmacological doses (10^{-6} M) of ATRA effectively displace HDAC complexes from RARa portion of the PLZF::RARa fusion protein, but fail to remove HDACs associated with POZ/BTB domain of the PLZF::RARa gene, as shown in Figure 4 [24]

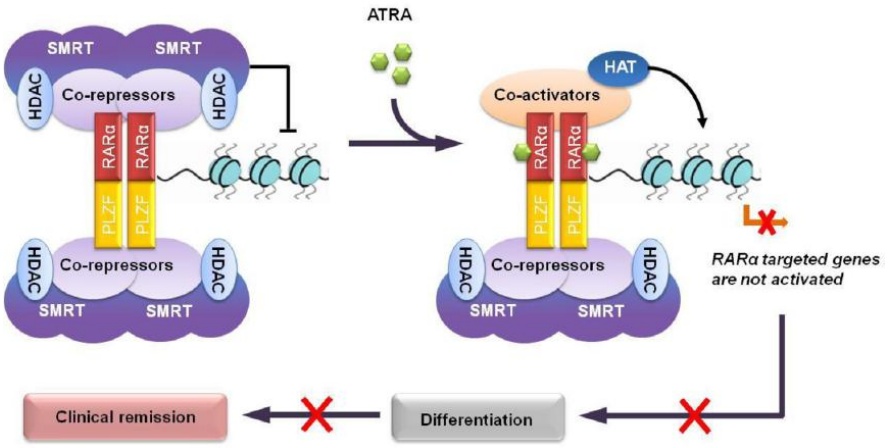

Figure 4. Schematic presentation of pathogenesis of PLZF::RARa-associated APL. Hussain L. et al., Seminars in Oncology, 2019.

The poor therapeutic response is attributed to the interaction between the PLZF portion of the fusion protein and nuclear receptor co-repressors, which confers resistance to treatment[30]. Consequently, this fusion protein serves as a model of therapy resistance.

2.5 Cell Metabolism

The term metabolism (from the Greek word μεταβολή, metabole, meaning change) refers to the biochemical reactions necessary for cellular homeostasis and survival. They consist of catabolic processes to produce energy and anabolic processes to synthesize macromolecules. The pathways involved in energy production in the body are: glycolysis, tricarboxylic acid cycle (TCA) cycle, β-oxidation of fatty acids (FAO), and oxidative phosphorylation (OXPHOS). Under normal conditions, glycolysis-derived pyruvate sustains the mitochondrial TCA cycles for the generation of Nicotinamide Adenine Dinucleotide (NADH) and Flavin Adenine Dinucleotide (FADH) and feeds the metabolic chain of NADH, Electron Transport Chain (ETC) and OXPHOS. In addition, fatty acids act as an energy source through β-oxidation to form acetyl-

CoA and reduced cofactors. Cellular metabolism changes depending on intrinsic signals and environmental changes. Otto Warburg noted, in 1956, that cancer cells tend to use aerobic glycolysis, generating lactate even in the presence of oxygen: the Warburg effect[31]. The withdrawal of the Pasteur effect (the inhibition of lactate generation in the presence of oxygen) in tumors became known as the Warburg effect, and for several decades the search for permanent, transmissible injuries to mitochondrial respiration that could support Warburg's hypothesis has not yielded conclusive results. Feodor Lynen for first hypotezing that uncoupling respiration to the formation of ATP could also result in the reversal of the Pasteur effect (Lynen, 1951). In this scenario, respiratory damage need not be an absolute requirement. Recent observations [32] have confirmed the inversion of the Pasteur effect with 2,4-dinitrophenol in human cells, also depending on the cellular landscape. Although, this agent produces a rapid increase in oxygen consumption, the chronic exposure may not lead to increased oxygen demand. Therefore, mitochondrial uncoupling could effectively mimic the Warburg effect in the absence of permanent and transmissible alterations in the oxidative capacity of cells. Gatenby and Gawlinski then suggested that the proglycolytic phenotype of solid tumors is, in fact, the result of environmental selection and provides tumor cells with an advantage for survival under the conditions of hypoxia and inflammation typical of premalignant lesions[33].

2.6 Metabolic Regulation of Hematopoietic Stem Cells (HSCs)

Hematopoietic stem cells (HSCs) predominantly exhibit a glycolytic metabolism. This metabolic peculiarity supports stem cell quiescence, limits the ROS generation, and preserves genomic integrity. After activation and commitment to differentiation, rapid switch from glycolysis to mitochondrial OXPHOS occurs. This metabolic reprogramming is essential to accommodate the increased bioenergetic and biosynthetic demands of lineage-committed

progenitors. This switch is accompanied by an elevation of ROS, activation of mechanistic target of rapamycin kinase (mTOR), enhanced mitochondrial biogenesis, and increased oxygen consumption. These changes support the high proliferative capacity and metabolic requirements of differentiating cells[2].

2.7 Metabolic reprogramming and dysregulated metabolism in LCS

Compared with HSCs, leukemic stem cells (LSCs) undergo a profound metabolic alterations that allows uncontrolled proliferation and resistance to apoptosis[34].
The environmental conditions provide the selective pressure for this adaptation, and we have seen significant changes in the dependence of AML cells on carbohydrates, amino acids and lipids, and significant changes in the way how these metabolites are processed within the preformed circuits of metabolism.
Enhanced consumption of metabolites like glucose[35, 36], glutamine [37, 38] and FAs [39] is one gain that helps AML cells to divide more rapidly than their normal counterparts, and to evade the apoptotic stimuli. Metabolic reprogramming such as the 'Warburg effect' is a common phenotype in cancer cells that allows their adaptation to the high metabolic demands necessary for sustaining their high rate of growth and proliferation. An enhanced glucose catabolism provides the rapid production of ATP and intermediates for the synthesis of nucleotides, amino acids and lipids[40].
LSCs exhibit a high dependence on mitochondrial OXPHOS[41], that provide a more efficient and sustained energy supply to support their survival and proliferation under stress conditions. This dependence on OXPHOS imposes a delicate balance: LSCs must tightly regulate their ROS levels to avoid oxidative stress, while taking advantage of mitochondrial metabolism[42]. Oncogenic mutations such as FLT3-ITD, BCR-ABL, and RAS drive metabolic rewiring and contribute to both increased ROS production and altered nutrient utilization[42], while anti-apoptotic proteins MCL-

1 and metabolic regulators like hexokinase II (HK2) stabilize mitochondrial function[39].
Clonal evolution further complicates the metabolic landscape, as AML cells dynamically adapt to environmental pressures by modulating their nutrient dependencies. Sujobert et al. [43]demonstrated that the mechanistic target of rapamycin complex 1 (mTORC1) hyperactivation renders AML cells selectively vulnerable to AMP-activated protein kinase (AMPK) activation, while targeting glutamine metabolism shows anti-leukemic activity[43]. Additionally, enzymes like PKM2 (M2 isoform of pyruvate kinase) and LDHA (lactate dehydrogenase A), which catalyze key steps in aerobic glycolysis, play central roles in supporting rapid cell division and metabolic adaptation[44, 45]. LDHA, in particular, is transcriptionally regulated by oncogenic drivers such as c-Myc and HIF-1α and has been linked to poor prognosis and drug resistance[46]. Deletion of PKM2 or LDHA impairs leukemogenesis in BCR-ABL and MLL-AF9 models[47]. Moreover, glyceraldehyde-3-phosphate dehydrogenase (GAPDH), beyond its classical role in glycolysis, has been implicated in the regulation of autophagy and cell survival in response to metabolic stress[48]. Therapeutic strategies targeting these dependencies, such as venetoclax, have demonstrated clinical efficacy, underlining the therapeutic potential of metabolic therapies.

2.8 ROS and mitochondrial damage

Mitochondria dysfunction and elevated oxidative stress contribute to AML[49, 50]. Alterations in mitochondrial capacity, imbalances OXPHOS and ETCs, become key generators of ROS within the cell[51]. ROS encompass a diverse group of small reactive oxygen-containing species, including superoxide anion, H_2O_2, hydroxyl radical, and NO; they are formed as by-products of normal metabolism and have oxidizing potential. In healthy hematopoiesis, ROS serve as signaling molecules. HSCs are able to self-replicate, continuously generating blood cells. During normal development,

regulated ROS levels stabilize the HSCs. In the hypoxic bone marrow microenvironment, quiescent HSCs maintain low ROS to safeguard their genomic integrity and support self-renewal. Exposure of HSCs to the oxygen-rich circulation increases ROS production, which in turn drives their activation, proliferation, and lineage commitment.
When HSCs are mobilized into the oxygen-rich circulation, increased ROS levels trigger their activation, leading to increased cell division and commitment to differentiated lineages. Aberrant ROS levels, a condition referred to as oxidative stress, can induce oxidative damage to both nuclear and mitochondrial DNA, impair DNA repair mechanisms, and increase cell mutation [49]. In addition, ROS can act as secondary messengers that sustain oncogenic signaling pathways, thereby contributing to the transformation and maintenance of the leukemic phenotype. In acute myeloid leukemia (AML), oxidative stress promotes a pro-leukemic environment through multiple mechanisms: genomic instability, epigenetic alterations, and metabolic reprogramming[52]. Therefore, intracellular ROS levels are tightly regulated by antioxidant system.

2.9 Antioxidant system

Several transcription factors regulate the expression of genes that are involved in antioxidant defense system in response to redox alterations. NRF2 (NF-E2 p45-related factor 2) is a master regulator of cellular resistance to oxidative stress. When stimulated, NRF2 dissociates from suppressor protein Keap1 (Kelch-like ECH-associated protein 1) in the nucleus and interacts with AREs (antioxidant response elements) to regulate the expression of cytoprotective genes, including HO-1 (heme oxygenase 1 gene), capable of neutralizing the heme group, which is highly cytotoxic by producing free radicals [53, 54] and G6PDH (glucose-6-phosphate dehydrogenase)[55]. In PML::RARa associated APL the transcriptional action of NRF2 is impaired by the fusion protein[56].

G6PDH, the rate-limiting enzyme in the pentose phosphate pathway, is responsible for the production of nicotinamide adenine dinucleotide phosphate (NADPH), a crucial cofactor for various anti-oxidant enzymes including superoxide dismutase (SOD) and catalase (CAT)[57]; SODs, with NADPH as a cofactor, catalyze the dismutation of the superoxide anion into hydrogen peroxide. This hydrogen peroxide is then transformed by CAT into water and molecular oxygen, a process that also requires NADPH[58]. Sirtuin 1 (SIRT1), a NAD+-dependent deacetylase, participate in glucose metabolism and lipid metabolism interacting with metabolism-related genes and contribute to cellular tolerance to oxidative stress by regulating many genes. Notably, SIRT1 activates NRF2 by changing the structure of Keap1, leading to NRF2 nuclear transfer and promoting the expression of antioxidant genes[59]. A family of SIRT targets are class O mammalian forkhead transcription factors, including FoxO3, which participate in regulating oxidative stress. SIRT1 is associated with the augmented deacetylation and activity of FoxO3a, which increased transcription of the mitochondrial antioxidant manganese superoxide dismutase (MnSOD) and CAT[60, 61].

2.10 Emerging drugs targeting oxidative stress to suppress AML

Targeting the altered redox balance of leukemic stem cells (LSCs) represents a therapeutic opportunity. By increasing intracellular ROS levels, pro-oxidant strategies can impair the antioxidant defenses that support LSC survival and resistance to chemotherapy, thereby improving chemosensitivity. However, excess ROS can also compromise the quiescent state and self-renewal capacity of normal hematopoietic stem cells (HSCs). AML cells exhibit a heightened vulnerability to oxidative stress compared to normal progenitor cells. This susceptibility is attributed to their low spare reserve capacity in the respiratory chain, rendering them more sensitive to oxidative damage. This AML vulnerability is further enhanced by the combined treatment with high-dose ascorbic acid (ASC) and

arsenic trioxide (ATO). At physiological concentrations, ASC enhances the efficacy of hypomethylating agents (HMAs) by promoting DNA demethylation, thereby contributing to the selective elimination of malignant cells[62, 63]. Ascorbate (ASC) exerts dose-dependent effects: at physiological concentrations it mainly acts as an antioxidant, whereas at pharmacological concentrations it switches to a pro-oxidant activity. In AML, high-dose ASC increases oxidative stress and ROS accumulation, triggering apoptosis of leukemic cells. This pro-oxidant effect has shown cytotoxic activity in vitro, particularly when combined with arsenic trioxide (ATO), both in AML cell lines and in primary patient blasts. [64]. These dual properties make ascorbic acid as a promising adjuvant in epigenetic therapies, with growing interest in its application in leukemia malignancies[65]. ATO further impairs antioxidant systems, such as thioredoxin reductase[66], amplifying ROS accumulation and cell death.

Another redox-targeting approach involves venetoclax, a selective BCL-2 inhibitor. In addition to disrupting anti-apoptotic signaling, venetoclax impairs OXPHOS, increasing mitochondrial ROS production and leading to LSC apoptosis. The combination of venetoclax with hypomethylating agents (HMAs) such as azacitidine or decitabine enhances these effects, particularly in $CD34^+$ AML cells with high drug resistance[67]. With the exception of some rare subtypes, APL is considered a curable disease, due to its remarkable sensitivity to ATRA and ATO. These agents target the fusion oncoprotein PML::RARa by binding to its respective moieties. In particular, ATO promotes the reformation of nuclear matrix-associated PML nuclear bodies (NBs) from PML::RARa multimers, ultimately leading to their proteasomal degradation (30). However, the ATRA and ATO efficacy is markedly reduced in the APL-like subtype characterized by the presence of the PLZF::RARa fusion protein. This limitation underscores the need for alternative therapeutic strategies. One promising avenue is the pro-oxidant approach, which aims to increase ROS levels to potentially improve treatment outcomes in AML.

2.11 Epigenetic landscape in AML

Epigenetic mechanisms are fundamental to both normal and malignant hematopoiesis. These modifications represent a category of heritable changes in gene expression that occur during cell division without altering the underlying DNA sequence. Persistent epigenetic alterations affecting transcription factors and chromatin-modifying enzymes activities play a key role in the onset and progression of hematologic malignancies[68]. Epigenetic modifiers represent a heterogeneous group of proteins, including DNMT3A, TET2, IDH1/2 and EZH2, responsible for the regulation of gene expression through DNA methylation at cytosine residues and post-translational modifications of histones, such as acetylation and methylation[69]. The deregulated epigenome of AML is closely linked to cellular metabolism and redox state. Several metabolic intermediates serve as essential cofactors for epigenetic enzymes: α-ketoglutarate (α-KG) supports the activity of TET DNA demethylases, while acetyl-CoA fuels histone acetyltransferases (HAT). Mutations in IDH1/2 disrupt the metabolism of α-KG, leading to the production of the oncometabolite 2-hydroxyglutarate (2-HG), which competitively inhibits TET enzymes and results in aberrant DNA hypermethylation and blocked differentiation[70]. Similarly, NAD^+, essential for sirtuin histone deacetylase activity, links redox balance to chromatin regulation[71]. DNA damage caused by oxidative stress impacts the epigenetic landscape, recruiting chromatin modifiers and leading to epigenetic reprogramming. In APL driven by PLZF::RARa, the fusion protein maintains a repressive chromatin state by recruiting histone deacetylases (HDACs) and polycomb group proteins on target genes, thereby silencing retinoic acid-responsive genes essential for myeloid maturation[72]. Given the reversible nature of epigenetic modifications, targeted therapies such as DNA methyltransferase inhibitors (DNMTis), like azacitidine (AZA), have attracted growing interest[73, 74].

2.12 Nuclear microRNAs act as Epigenetic Modulators inHematopoiesis and Leukemia

MicroRNAs (miRNAs) are small noncoding RNAs of about 19 to 24 nucleotides that regulate gene expression primarily through base pairing with complementary sequences in target mRNAs, leading to translational repression of the mRNA. miRNAs influence multiple biological processes, including cell fate, proliferation, differentiation, and apoptosis. Altered regulation of miRNAs by oncogenic proteins plays a critical role in the pathogenesis of leukemia. miRNAs regulate gene expression post-trascriptionally by either inhibiting protein translation or inducing mRNA degradation, depending on whether they bind imperfectly or perfectly respectively to the 3-untranslated regions (3'-UTRs) of their target mRNAs[75]. These functions of miRNAs take place in the cell cytoplasm through their binding to mature mRNAs. However, recent discoveries have extended the functional repertoire of miRNAs to include their regulatory activities within the nucleus [76]. Nuclear miRNAs can bind to complementary DNA sequences within gene promoters, thereby contributing to transcriptional regulation. This activity often involves the recruitment of chromatin-modifying complexes, directly shaping the epigenetic landscape of target loci. Depending on the context, nuclear miRNAs can induce transcriptional activation or repression. The outcome of these interactions is influenced by several factors, including the presence of CpG islands and TATA boxes[77]. In the hematopoietic system, miRNAs are expressed in a tightly regulated and lineage-specific manner and are essential for maintaining the balance between self-renewal and differentiation[78]. Alterations in miRNA expression can disrupt this balance, contributing to leukemogenesis [79]. In AML, aberrant epigenetic reprogramming plays a central role in disease progression[80]. The discovery of the functions of nuclear miRNAs expands our understanding of how noncoding RNAs can enhance epigenetic states that promote therapy resistance.

3. AIM

Acute Myeloid Leukemia (AML) is a highly heterogeneous disease characterized by the disruption of normal hematopoiesis due to genetic, epigenetic, and metabolic alterations. While extensive studies have improved our understanding on the molecular drivers of AML, therapeutic outcomes remain unsatisfactory, due to the persistence of leukemic stem cells (LSCs), clonal evolution, and therapy resistance.

Cellular metabolism and redox homeostasis play a pivotal role in supporting leukemic transformation. Aberrant metabolic reprogramming allows AML cells to adapt to nutrient availability and sustain high proliferative demands.

Hematopoietic stem cells rely primarily on glycolysis to maintain quiescence and genomic integrity through low ROS levels, whereas LSCs undergo metabolic rewiring toward OXPHOS and enhanced nutrient flexibility.

Targeting metabolic pathways, mitochondrial function, or redox regulators selectively impairs LSC survival, highlighting the therapeutic potential of metabolic vulnerabilities in AML.

Epigenetic deregulation is a hallmark of AML, driven by mutations in chromatin modifiers and reinforced by altered metabolic intermediates. Oxidative stress and DNA damage dynamically remodel the epigenetic landscape. Nuclear microRNAs emerge as epigenetic regulators, that interact with chromatin and regulate transcription in normal and aberrant hematopoiesis. The overall goal of the PhD project is to link chromatin organization and metabolism to normal and aberrant myeloid differentiation to identify therapeutic potential targets for the treatment of AML. We studied the metabolism in normal hematopoietic progenitors/precursors (HP/Ps) undergoing myelopoiesis and in fully characterized AML blasts from a large number of patients. Furthermore, the project aims to explore metabolic alterations in cellular models expressing the PLZF::RARa fusion protein, with a particular focus on evaluating its impact on the cellular redox balance and antioxidant systems. The

major points of the project involve: (i) to identify the landscape of metabolic regulation during human myelopoiesis and in AMLs; (ii) to study the changes in expression patterns of metabolic genes transcriptionally regulated in normal and leukemic hematopoietic cells and the role of PLZF::RARa and nuclear miR-223; (iii) to characterize and functionally validate the selected metabolic genes and pathways in normal and neoplastic hematopoiesis; (iv) to identify and pre-clinically test potential therapeutic approaches based on compounds targeting the identified genes.

4. RESULTS

4.1 Characterization of the metabolic capacity in normal myeloid progenitors and AML blasts

We analyzed the landscape of metabolic regulation during human myelopoiesis and in AMLs, by evaluating the metabolic peculiarities of normal bone marrow cells (NBM), early progenitors/precursors (EP/P) and primary AML blasts from 19 patients.

By using, the Seahorse Bioscience XFe96 analyzer, we measured the oxygen consumption rate (OCR) and extra cellular acidification rate (ECAR). The basal glycolysis, glycolytic reserve and glycolytic capacity in AML blasts were higher than in NBM. However, AML blasts showed lower basal glycolysis ($p = 0.01$), glycolytic capacity ($p = 0.02$) and glycolytic reserve ($p = 0.06$) than early progenitors/precursors (EP/P) derived from CB CD34+ cells at day 7 of culture (N7, mostly promyelocytes: CD11b+ 16.8%, CD13+ 86.6%, CD14+ 5.1%, CD15+ 3.2% and CD34+ 45.2%) whereas these values were comparable between AML blasts and EP/P at day 13 of culture (N13, mostly granulocytes: CD11b+ 72%, CD15+ 80% and CD34+ 7%) (Fig. 5A).

Concerning mitochondrial respiration, the level of oxidative phosphorylation (OXPHOS) is greater in AML blasts than in NBM. We found that a group of AML blasts with higher OXPHOS ($n = 7$, 54 ± 12 pmol/min/ × 105 cells) showed similar values to those of EP/P (N7), whereas the group of AML with lower OXPHOS ($n = 12$, 16 ± 6 pmol/min/ × 105 cells; $p < 0.0001$) could be compared to those of EP/P (N13) (Fig. 5B). As a consequence of increased OXPHOS, increased energy production (ATP) (Fig. 5C) and proton leak (PL) levels (Fig.5D) were observed. The lower spare respiratory capacity (SRC) values observed in AML blasts compared to EP/P promyelocytes (N7) ($n = 19$, 74 ± 49 vs. $n = 3$, 153 ± 54 pmol/min/×105 cells) ($p = 0.02$) denoted their higher susceptibility to oxidative stress (Fig.5E).

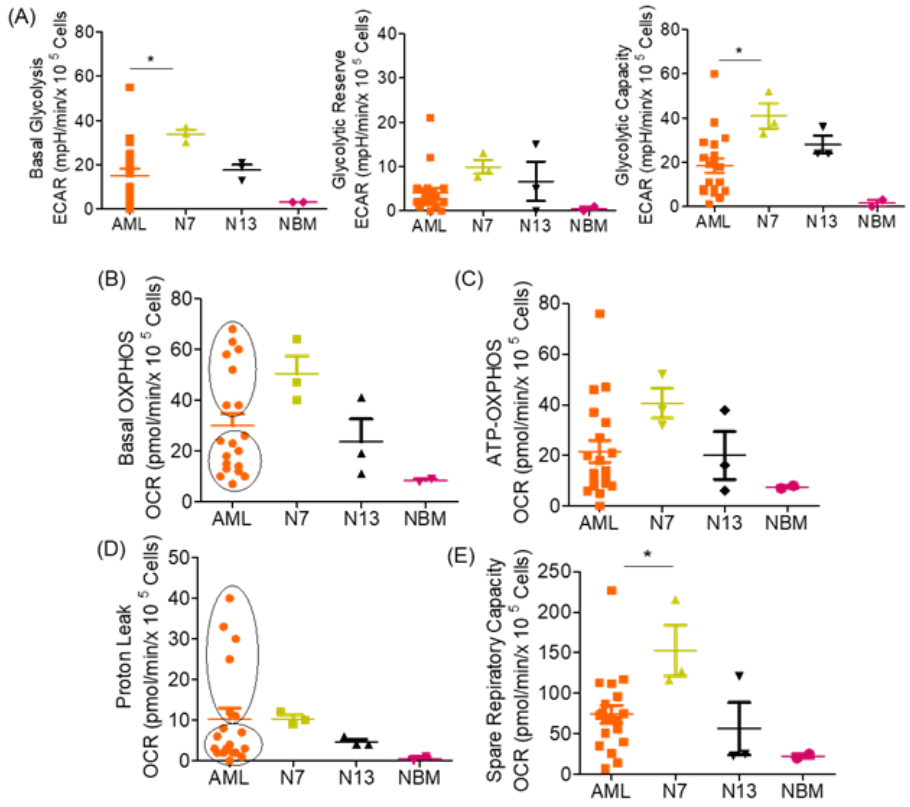

Figure 5. Measurements of glycolytic rates in primary blast from AML patients, EP/P at day 7 (N7, mostly promyelocytes) and at day 13 (N13 mostly neutrophils) and normal bone marrow (NBM). Histograms represent (A) basal glycolysis, glycolytic reserve and glycolytic capacity. (B) basal respiration, (C) ATP, (D) PL and (E) spare respiratory capacity (SRC). Statistical analysis was performed using the nonparametric Mann–Whitney t test, two-sided The distribution of the samples was not normal. *$p \leq 0.05$, **$p \leq 0.00$.

Kaplan Mayer analysis showed that AMLs with higher PL levels had significantly shorter overall survival (OS) than AMLs with lower PL levels (OS, median = 1 vs 16 months, p = 0.047). The group of AMLs with high SRC showed a trend of shorter OS time

than the group of AMLs with low SRC (OS, median = 7 vs 16 months), (p = 0.1) (Fig. 6). These results indicated that high PL levels and high SRC values are associated to high basal respiration and confer aggressiveness and resistance to therapy to AMLs.

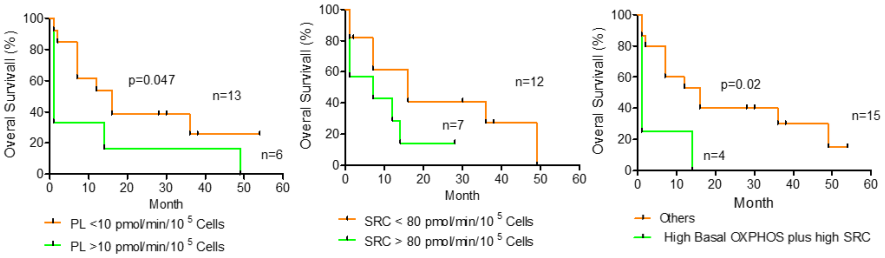

Figure 6. AML patients with high mitochondrial respiration show worse overall survival. Kaplan–Meier plots for overall survival (OS) in AML patients' groups stratified according to high and low levels of:(left) PL (cut off 10 pmol/min/105 cells), (middle) SRC (cut off 80 pmol/min/105 cells), (right) high basal OXPHOS plus high SRC (basal OXPHOS cut off 35 pmol/min/105 cells). The tick marks indicate the times at which events (death for OS or relapse, induction death, death in complete remission or second tumor for EFS) were recorded. Statistical analysis was performed using the Log-rank (Mantel–Cox) test. *p ≤ 0.05, **p ≤ 0.005.

4.2 PLZF::RARa promotes Mitochondrial Metabolism

Acute myeloid leukemia (AML) is characterized by altered cellular metabolism, with a strong reliance on mitochondrial function. We evaluated Mitochondrial Respiration, measuring the oxygen consumption rate (OCR) in primary blast from a patient with APL carrying the PLZF::RARa fusion.

PLZF::RARa+ blasts show basal mitochondrial respiration comparable to that observed in early progenitors/precursors (EP/P) derived from CB CD34+ cells at day 7 of culture (EP/P N7, mostly promyelocytes). However, basal respiration in PLZF::RARa+ blasts was higher than that measured in EP/P at day 13 of culture (EP/P N13 predominantly granulocytes).

In contrast, APL blasts carrying the PLZF::RARa fusion exhibited lower spare respiratory capacity (SRC) than that measurable in

normal promyelocytes EP/P (N7) and in more differentiated granulocytic precursors EP/P (N13), a feature that may render leukemic cells more susceptible to oxidative stress.
This reduction in SRC was accompanied by an increase in proton leak (PL) in PLZF::RARa-positive APL-like blasts if compared with both EP/P (N7) and EP/P (N13) cells, and by a decreased ATP production relative to EP/P (N7), though remaining higher than in EP/P (N13) cells (Fig. 7 and Table 2).

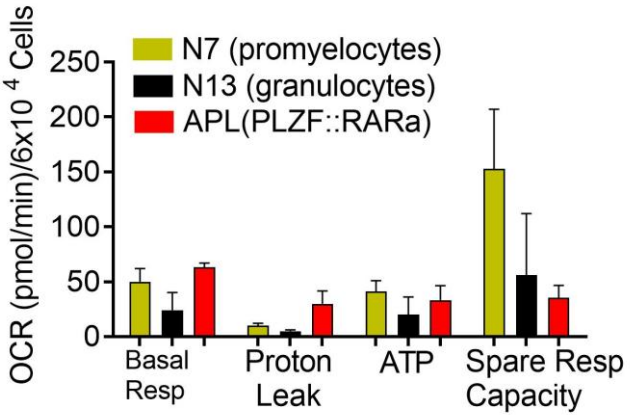

Fig. 7. Characterization of PLZF::RARa-positive APL-like primary blast and N7 promyelocytes and N13 granulocytes (early progenitors/precursors EP/Ps) mitochondrial metabolism. Histograms represent: Basal respiration, proton leak (PL), mitochondrial ATP and spare respiratory capacity (SRC). Data are presented as mean ± SD of three independent measurements per group.

		EP/P (N7)	EP/P (N13)	APL PLZF::RARa
Mitochondrial Respiration	**Basal**	50±12	24±16	63±4
OCR(pmol/min/105 Cells)	**SRC**	114±58	56±56	35±11,3
	PL	10±2	5±1	30±12
	ATP	41±10	20±16	33±13

Table 2. Mitochondrial respiration values in PLZF::RARa-positive APL-like primary and normal hematopoietic cells. OCR (oxygen consume rate); EP/P (early progenitors/precursors; N7 (at day 7); N13 (at day 13); SRC (spare reserve capacity); PL (Proton Leak). Values represent the mean ± SD.

We first observed that AML patients with high OXPHOS activity and high PL levels have a particularly poor prognosis. Building on this finding, we focused on PLZF::RARa-positive APL-like patients, who also display elevated OXPHOS and PL levels. This subgroup can therefore serve as a valuable model to investigate the link between these metabolic features and adverse outcomes in AMLs. Therefore, we performed the same analyses in a PLZF::RARa-inducible cell model described in the method section. Zinc-induced PLZF::RARa expression in B412 cells increases mitochondrial respiration: basal oxidative phosphorylation (OXPHOS) (MT:95±6 B412:135±14 (pmol/min)/6x104 cells), $p<0.0001$), respiratory reserve (MT:93±41 B412:155±55 (pmol/min)/6x104 cells), $p=0.01$) and ATP production (MT:65±20 vs B412:96±23 (pmol/min)/6x104cells), $p=0.008$)] (Fig. 8A). Western blot analysis confirmed the expression of the PLZF::RARa fusion protein upon zinc treatment in B412 up to 24 hours, providing evidence that fusion protein induction supports the observed metabolic phenotype (Fig. 8B).

To assess the relative contribution of different metabolic fuels, such as glucose, fatty acids, and glutamine, to mitochondrial respiration, we performed substrate oxidation tests, providing insights into the metabolic flexibility and substrate dependency of the cells. Under

basal conditions, PLZF::RARa+ B412 cells exhibited a greater capacity to utilize diverse metabolic substrates compared to MT controls (Fig. 9A). Both these cell types showed a sensible increase in reliance on fatty acid oxidation following etomoxir (ETO) treatment. ETO is an irreversible inhibitor of carnitine palmitoyltransferase 1a (CPT1a), an outer mitochondrial membrane enzyme required for the transport and oxidation of long-chain fatty acids (LCFA) within mitochondria. Notably, following PLZF::RARa expression, the acute cell response to ETO was greater in MT cells compared to B412 cells, indicating that PLZF::RARa expression reduces dependency on LCFA and confers greater metabolic flexibility, allowing enhanced utilization of pyruvate and glutamine (Fig. 9B). The most pronounced maximal response was detected in the presence of PLZF::RARa, regardless of whether glucose, glutamine, or LCFA oxidation was inhibited (Fig. 9C).

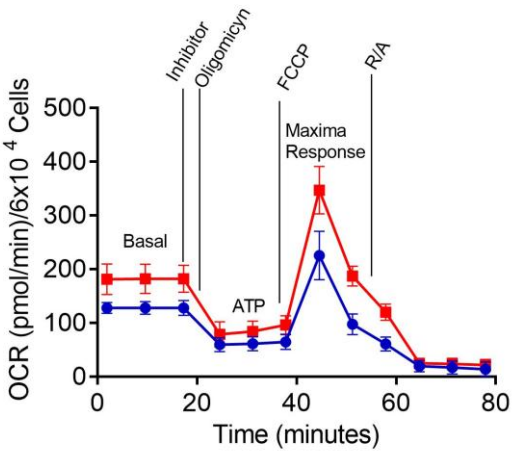

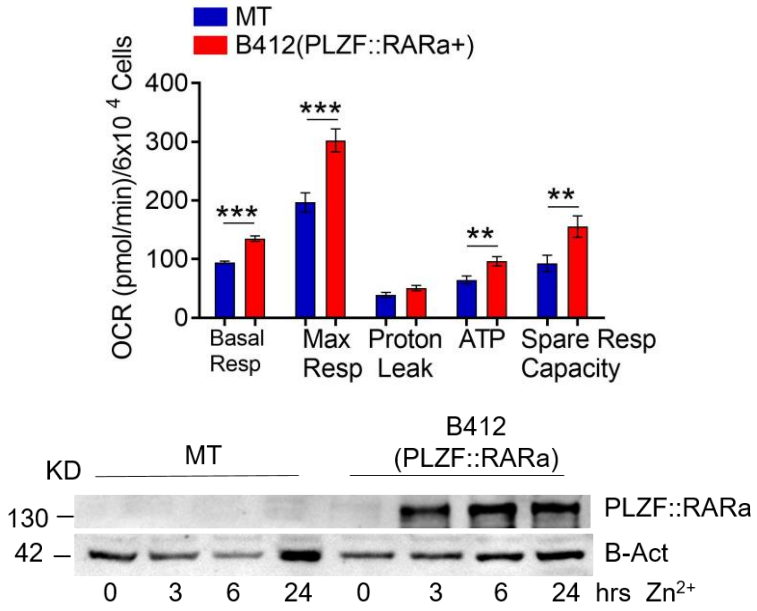

Figure 8. Characterization of mitochondrial metabolism in PLZF::RARa+ B412 and control MT cell lines. (A) Histograms represent basal respiration, maximal respiration, PL, mitochondrial ATP and SRC capacity measured using the XF Myto Stress Test assay. The statistical analysis was performed using Student's t-test. Basal oxidative phosphorylation (OXPHOS) ***: $p<0.0001$, Respiratory reserve **: $p=0.01$ and ATP production **: $p=0.008$ (B) Western blot analysis confirming zinc-induced expression of the PLZF::RARa fusion protein in B412 cells up to 24 hrs.

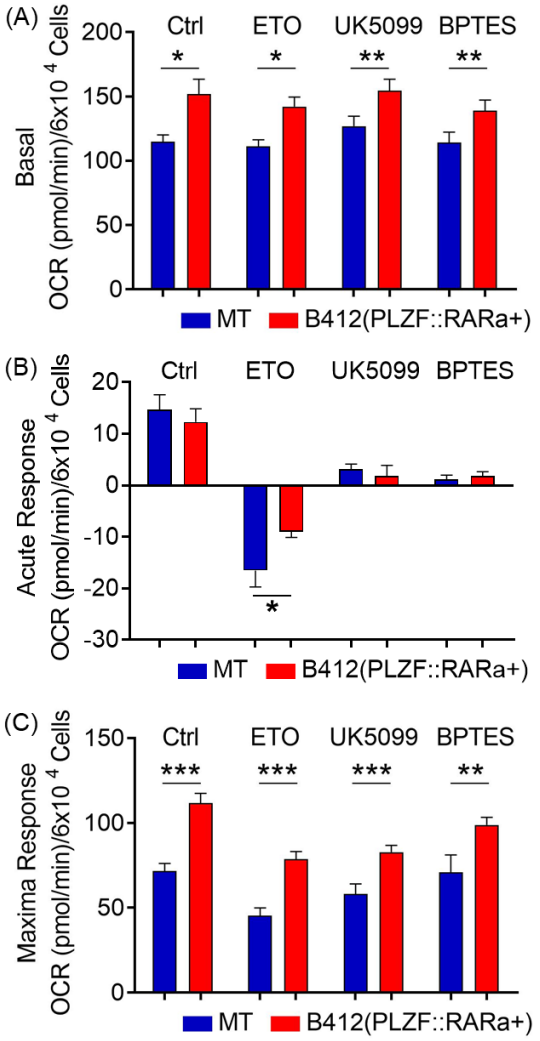

Figure 9. Evaluation of the mitochondrial fuel usage in MT control cells and in B412 cells expressing PLZF::RARa using the XF Mito Fuel Flex Test. The statistical analysis was performed using Student's t-test. The graphs shown (A) Basal Response: Ctrl *p=0.04, ETO *:p=0.02; UK5099 **p=0.005; BPTES **: p=0.003 (B) Acute Response: ETO *:p=0.04; and (C) Maxima Response: Ctrl ***: p=0.0001, ETO ***: p=0.000; UK5099 ***: p=0.0000; BPTES **: p=0.009.

PLZF::RARa expression in B412 cells was associated to a reduction in basal glycolysis (Basal Glycolysis MT: 93±41 B412: 155±55 (pmol/min)/6x104 cells), p=0.01) (Fig. 10).

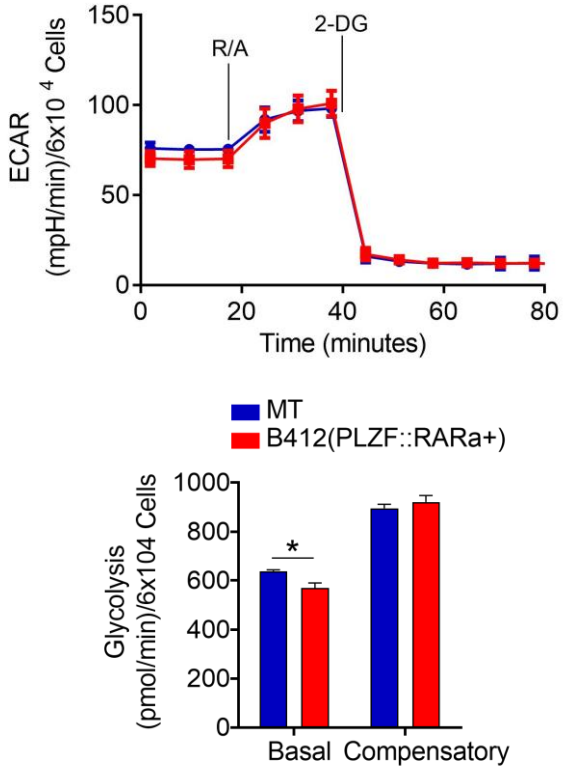

Figure 10. Characterization of PLZF::RARa+ B412 cell lines glycolytic metabolism. Histograms represent Basal glycolysis and glycolytic compensatory measured using the XF Glycolytic Rate Assay. The statistical analysis was performed using Student's t-test. Basal Glycolysis *: p=0.01.

In comparison to MT cells, B412 cells displayed a slightly higher mitochondrial ATP production (MT: 323±88 vs B412: 377±172 (pmol/min)/6x104 cells) and reduced glycolytic ATP (MT: 732±119 vs B412: 550±70 (pmol/min)/6x104 cells), p=0.01) (Fig. 11) (Table 2).

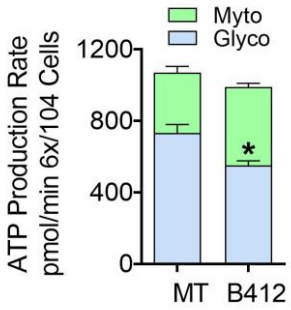

Figure 11. Characterization of ATP metabolism in PLZF::RARa+ B412 cell lines. XF real-time glycolytic and mitochondrial ATP production rate by the ATP Rate Assay. The statistical analysis was performed using Student's t-test *p=0.01

		MT+Zn	B412+Zn	p-value
Glycolysis ECAR(pmol/min/105	**Basal**	665±55	547±47	0.01
	Compensatory	868±61	857±99	
Mitochondrial Respiration OCR(pmol/min/105 Cells)	**Basal**	95±6	135±14	<0.0001
	SRC	93±41	155±55	0.01
	ATP	65±20	96±23	0.008
Basal Response OCR(pmol/min/105 Cells)	**Ctrl**	10±10	135±37	0.04
	ETO	109±14	129±26	0.024
	UK5099	123±21	155±22	0.005
	BPTES	115±18	143±21	0.003
Acute Response OCR(pmol/min/105 Cells)	**Ctrl**	10±10	11±7	0.944
	ETO	-15±7	-9±4	0.04
	UK5099	3,3±2,5	0,6±5,2	0.58
	BPTES	2±4	1±4	0.58
Maxima Response OCR(pmol/min/105 Cells)	**Ctrl**	61±19	103±21	0.0001
	ETO	43±11	75±12	0.000
	UK5099	53±16	83±12	0.000
	BPTES	65±26	93±23	0.009
ATP	**Glycolytic**	732±119	550±70	0.01
	Mitochondrial	337±87	337±172	0.62

Table 2 Mitochondrial respiration and Glycolysis in MT (Ctrl) and B412 (PLZF::RARa+) cells. Values represent the mean ± SD. Statistical analysis was performed using the Student's t-test.

These findings indicate that PLZF::RARa expression reprograms cellular metabolism, promoting enhanced mitochondrial function, increased substrate flexibility, and reduced reliance on glycolysis all mechanisms that may contribute to therapeutic resistance.

4.3 PLZF::RARa Expression Increases ROS Levels and Disrupts Antioxidant Defense

Increased mitochondrial activity is typically associated with elevated electron transport chain flux, which can lead to higher electron leakage and, consequently, augmented production of reactive oxygen species (ROS)[81].
Therefore, we quantified intracellular ROS levels in B412 and MT cells following 24 hours of exposure to $ZnSO_4$. Expression of PLZF::RARa in B412 cells disrupted the antioxidant balance, resulting in elevated ROS levels compared to control cells. Upon treatment for 2 hours with 3mM Ascorbate (ASC), which acts as a ROS inducer at high doses, ROS levels were higher in B412 cells than in MT cells (B412| 8058±568 vs MT| 5037±574; p=0,03). Similarly, exposure to Rotenone-Antimycin (positive control), inhibitors of mitochondrial electron transport, further increased ROS accumulation in B412 cells relative to MT cells (B412| 38148±1756 vs MT| 19588±2761; p=0,01). Conversely, treatment with N-acetyl-L-cysteine (NAC), an antioxidant and precursor of intracellular glutathione, was used as a negative control to validate the assay. NAC, supporting the cellular antioxidant defense system, neutralized ROS production in both cell lines (B412: 6060±1456 vs MT: 6067±444) (Fig.12). Collectively, these results indicate that PLZF::RARa expression promotes a redox imbalance by elevating ROS levels, likely due to compromised antioxidant defense mechanisms.

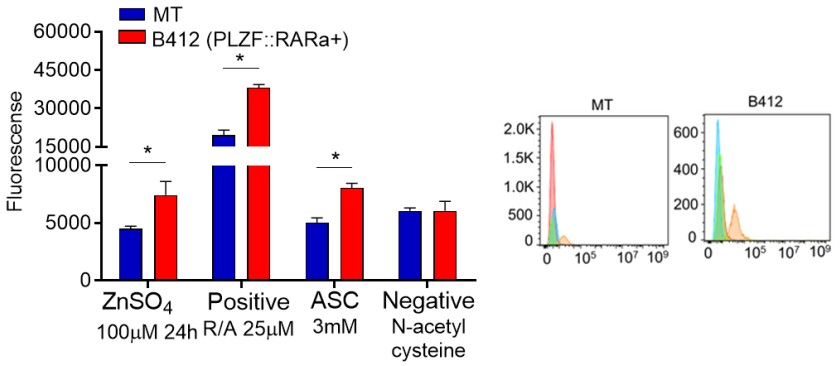

Figure 12. PLZF::RARa expression increases ROS production**.** ROS levels were measured in B412 expressing PLZF::RARa and control cells, using Rotenone/Antimicyn (positive control) and high dose ascorbate (ASC, ROS inducer). In all conditions, PLZF::RARa expressing cells exhibited significantly higher ROS levels compared with MT cells. The experiments were performed in triplicate. The statistical analysis was performed using Student's t-test. * p< 0,05; N= 2.

Based on this results, we investigated the role of PLZF::RARa in modulating the cellular defense against oxidative stress. We focused on NRF2, the master regulator of cellular redox homeostasis. Following treatment with 100 µM $ZnSO_4$, *NRF2* mRNA levels remained comparable between B412 and MT cells throughout the 24-hour period (MT 24h: 0.8±1.1 vs B412 24h: 1.6±1.0) (Fig. 13), indicating that the fusion protein does not significantly affect NRF2 transcription. Notwithstanding, NRF2 protein levels were lower in B412 cells than in control cells (MT 24h: 1.2±0.3 vs B412 24h: 0.3±0.1) ($p = 0.008$), indicating that PLZF::RARa impairs NRF2 protein stability (Fig. 14).

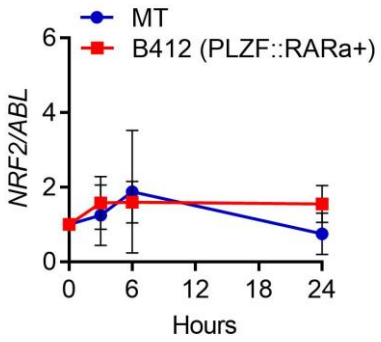

Figure 13. *NRF2* mRNA expression did not differ significantly between PLZF::RARa-induced and control conditions. The experiments were performed in quadrupled. The statistical analysis was performed using Student's t-test.

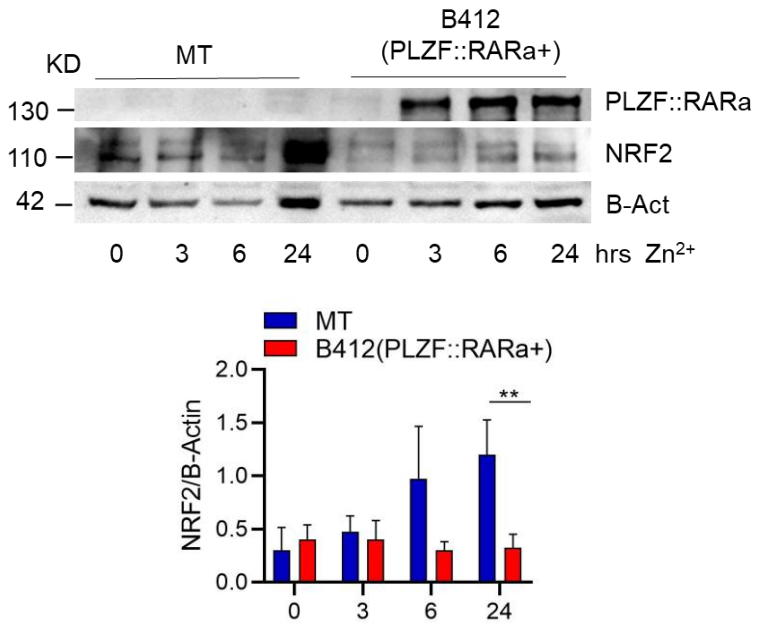

Figure 14. PLZF::RARa expression downregulate the NRF2 Protein. The NRF2 protein level increased and persisted higher in the 24 h after $ZnSO_4$ treatment in MT cells, but not in B412 cells expressing PLZF::RARa. The experiments were performed in quadrupled. **: p=0.008 by unpaired t-test by Welch's t-test.

NRF2 mRNA expression levels in PLZF::RARa-positive APL-like patients' samples (n=5: 0.5±0.5) were lower compared with NBM (n=5:1±0.4), PML::RARa APLs (n=15: 4.8±2.2) (p=0.004), and AML samples (n=14: 8.9±19) (p=0.02)(Fig. 15). These data suggest that PLZF::RARa may regulate NRF2 through a post-transcriptional mechanism.

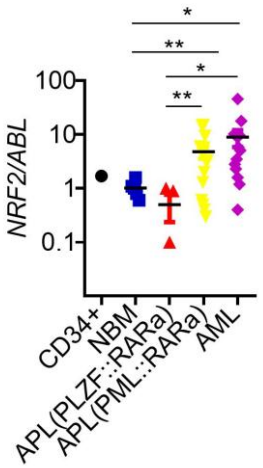

Figure 15. NRF2 mRNA expression in AML patient samples. Q-RT-PCR analysis of NRF2 mRNA in CD34+ (n=1), NBM (n=5), 4 PLZF::RARa-positive APL-like patients (n=4), PML::RARa-APL (n=15) and AML (n=14) samples. * p< 0,05; **: p <0.005 by unpaired t-test.by Welch's t-test.

Since NRF2 is a master regulator of the adaptive response to oxidative stress, its deregulation led to defective induction of downstream target genes. We measured in the same cell system the expression levels of NRF2 target gene HMOX1 (HO-1), a key antioxidant gene that normally plays a protective role in cancer cells. Consistent with reduced NRF2 protein levels, HO-1 expression was downregulated in PLZF::RARa+ B412 cells ($ZnSO_4$ 24 h: B412: 0.3 ± 0.3 vs. MT: 1.1 ± 0.8) (Fig. 16).

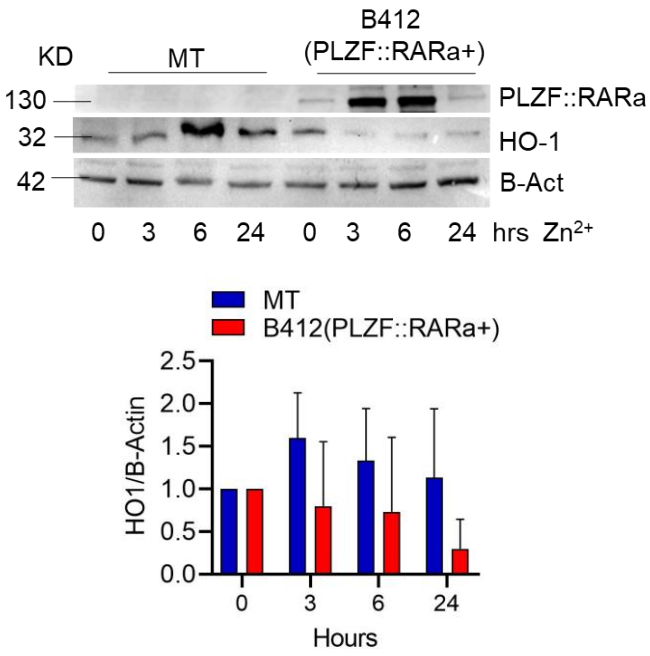

Figure 16. Evaluation of HO-1 protein levels in MT control cells and in B412 cells expressing PLZF::RARa. The experiments were performed in triplicate. The statistical analysis was performed by unpaired t-test by Welch's t-test.

We evaluated NRF2 transcriptional activity using quantitative PCR, analyzing basal levels of HO-1 transcript. This analysis showed a reduction in *HO-1* mRNA expression in the presence of the PLZF::RARa fusion oncoprotein 6 hours after treatment with $ZnSO_4$ (6 h: 1.7 ± 0.1 vs. MT: 3.6 ± 0.7; p = 0.01) (Fig. 17).

HO-1 mRNA expression levels in PLZF::RARa-positive APL-like patients (n=5: 0.5±0.3) were significantly lower than in NBM (n=11:1.4±1.3), PML::RARa APLs (n=14: 2.6±3.6) and AML (n=12: 39.7±43.7) (p=0.01) samples (Fig. 18).
The kinetics of NRF2 protein and induced expression of HO-1 are very similar, both being suppressed in the presence of PLZF::RARa.

This indicates that PLZF::RARa inhibits NRF2 activity, preventing the transcription of its downstream target HO-1.

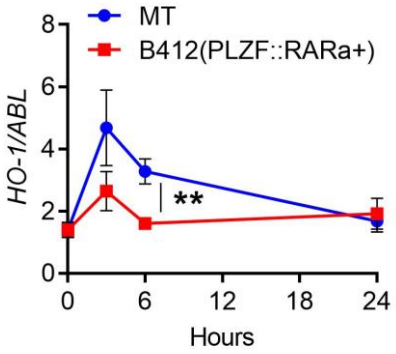

Figure 17. PLZF::RARa interferes with NRF2 Transcriptional Activity. PLZF::RARa inhibits NRF2 transcriptional activity in B412 cells, as shown by reduced *HO-1* mRNA expression. The experiments were performed in quintupled. **: p =0.01 by unpaired t-test by Welch's t-test.

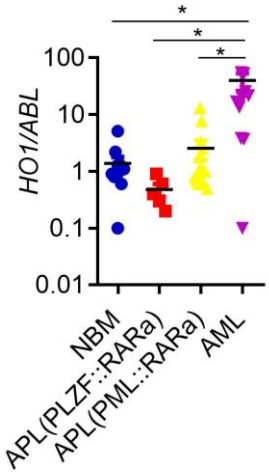

Figure 18. Evaluation of HO-1 expression in Primary Hematopoietic cells. mRNA expression of NRF2 target genes: HO-1 in 5 PLZF::RARa-positive APL-like, 14 APL, 12 AML and 11 normal bone marrow (NBM). * p=0.01 by unpaired t-test by Welch's t-test.

4.4 PLZF::RARa forms a Nuclear Complex with NRF2

To investigate the mechanism underlying NRF2 dysfunction, we examined its physical interaction with PLZF::RARa. Co-immunoprecipitation assays, performed using an anti-PLZF antibody for pulldown and probing with an anti-NRF2 antibody, revealed a physical interaction between PLZF::RARa and NRF2 in B412 cells (Fig. 19A and 19B).

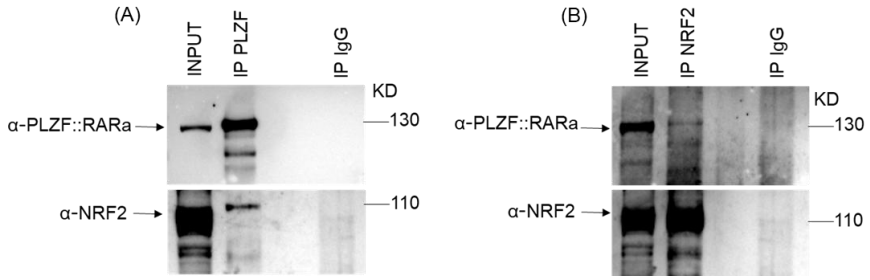

Figure 19. Co-immunoprecipitation assays for evaluating the interaction of PLZF::RARa with NRF2. B412 cells where treated with $ZnSO_4$ 100 µM for 6 hours, after that co-IP assays (IP: PLZF; WB: NRF2) showed that PLZF::RARa interacts with NRF2, and this binding was confirmed by reverse Co-IP assays (IP: NRF2; WB: PLZF).

Since the transcriptional function of NRF2 is nuclear we decided to examine the PLZF::RARa effect on the cellular localization of NRF2. By confocal microscopy we observed a significant increase in nuclear co-localization of NRF2 with PLZF::RARa in B412 cells compared to MT controls (Coeff Spearman MT: 0,4 vs B412: 0,6 ($p<0,0001$) (Fig. 20).

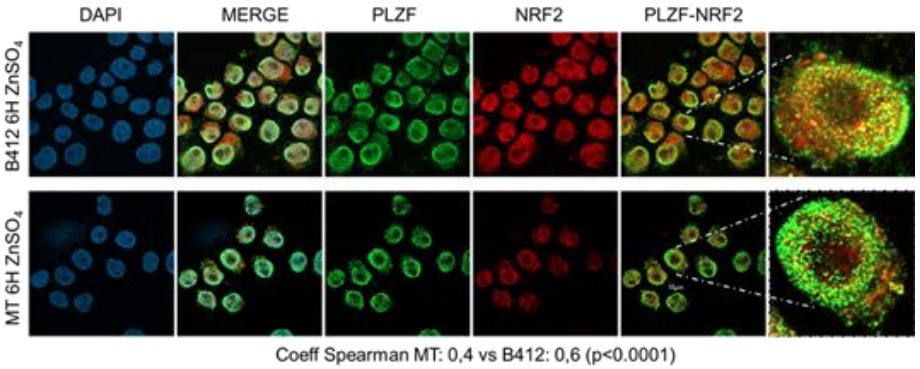

Figure 20. Interaction between PLZF::RARa and NRF2 in the nucleus of indicated cell lines by confocal microscopy

The PLZF::RARa-NRF2 nuclear association was confirmed by the Proximity Ligation Assay (PLA) assay (Fig. 21).

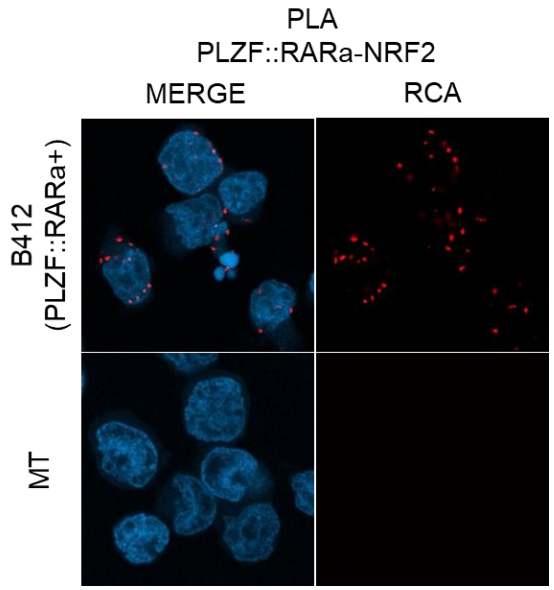

Figure 21. Detection of PLZF::RARa-NRF2 protein interaction by PLA assay in B412 cells. Control was performed by omitting the primary antibody. Red spot represents a single interaction between PLZF::RARa-NRF2.

We confirmed the subcellular localization of NRF2 protein by western blot analysis, separating nuclear and cytoplasmic cellular fractions. Western blot analysis of nuclear (Fig.22 top) and cytoplasmic fractions (Fig. 22 down) showed that NRF2 accumulated in the nucleus of B412 cells following PLZF::RARa expression (B412 6h: 0.9 ± 0.42 vs. MT: 0.4 ± 0.2; p = 0.03), while cytoplasmic levels remained unchanged (B412: 0.8 ± 0.5; MT: 0.8 ± 0.3). Together, these results indicate that PLZF::RARa binds NRF2 in the nucleus.

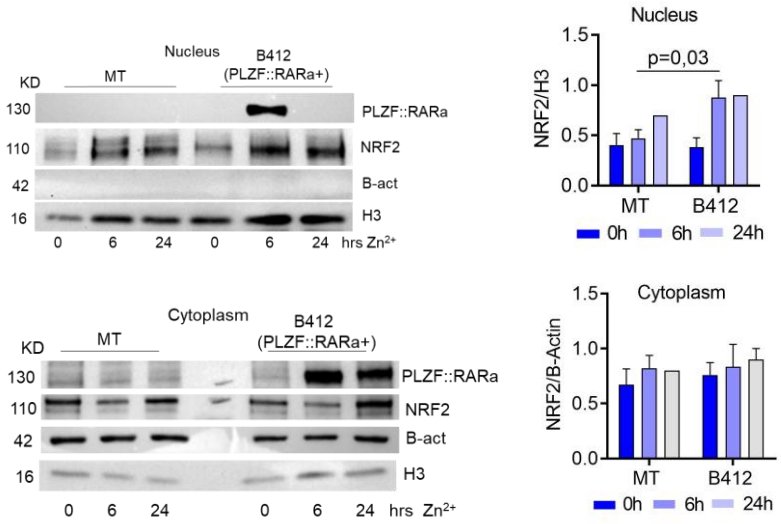

Figure 22. NRF2 nuclear translocation (up) in PLZF::RARa+ B412 cells is confirmed by nuclear/cytoplasmic fractionation. The experiments were performed in triplicated. The statistical analysis was performed using Student's t-test.

4.5 PLZF::RARa-mediated regulation of G6PDH expression

Given the critical role of G6PDH in maintaining redox homeostasis, sustaining NADPH production, we next investigated whether its expression was affected by PLZF::RARa. To assess whether

G6PDH expression is affected by PLZF::RARa, we analyzed *G6PDH* mRNA levels in blast samples from PLZF::RARa-positive APL-like patients (n=5 0.7±0.5), NBM (n=5: 1.6±1.2), PML::RARa APLs (n=10: 0.8±0.5), AML (n=7: 0.7±0.5). While the *G6PDH* levels were lower in AML blast if compared to NBM cells, no significant differences were observed among the groups. This may be due to the low number of samples (Fig. 23).

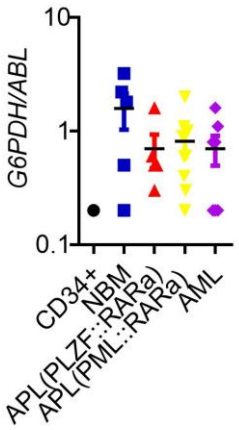

Figure 23. *G6PDH* mRNA level is lower in primary blast. Quantitative RT-PCR analysis of *G6PDH* mRNA was performed on 1 CD34+, 5 five normal bone marrow (NBM), 5 PLZF::RARa-positive APL-like samples, 5 PML::RARa-APL samples and 10 AML samples. The statistical analysis was performed by unpaired t-test by Welch's t-test.

In contrast, B412 cells expressing PLZF::RARa showed a significant reduction in *G6PDH* mRNA levels compared to control cells (B412 6 h: 0.65 ± 0.38 vs. MT 6h: 1.5 ± 0.2) (Fig. 24).
At the protein level, G6PDH expression in B412 cells progressively declined over 24-hour of $ZnSO_4$ addition (24h B412: 1.8±0.5 vs MT: 3.1±0.6, p=0.04) (Fig. 25).

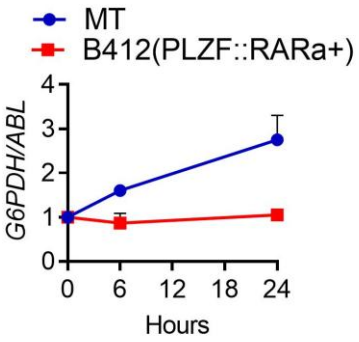

Figure 24. In PLZF::RARa+ B412 cell *G6PDH* mRNA expression was lower than in controls throughout the 24-hour $ZnSO_4$ induction time course.The experiments were performed in triplicate. The statistical analysis was performed by unpaired t-test by Welch's t-test.

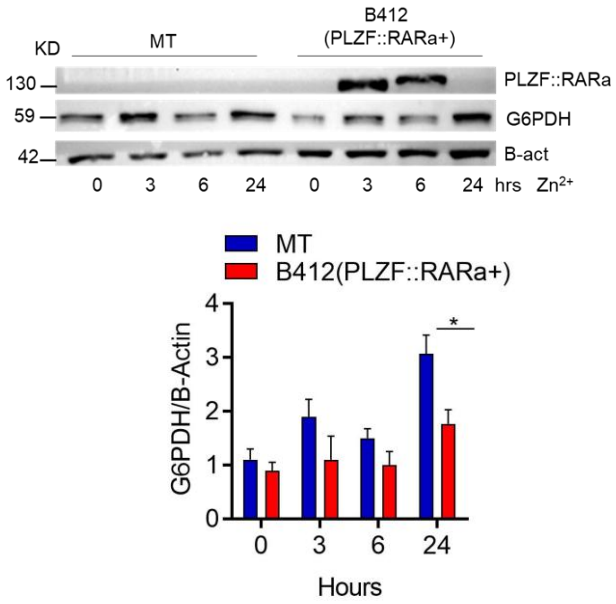

Figure 25. Analysis of G6PDH protein levels showed that its expression remained lower in PLZF::RARa-expressing cells compared with controls after 24 hours of treatment with 100 µM $ZnSO_4$. Statistical analysis was performed by unpaired t-test by Welch's t-test. *: p=0.04

We also observed lower NADPH production at 16 hours after fusion protein induction by $ZnSO_4$ treatment (Fig.26 left); however, at 6 hours, NADPH production was higher in B412 (Fig. 26 right). Quantification of NADPH levels in MT and B412 cells was performed using different cell numbers normalized to total protein content. However, due to the varying intracellular NADPH levels required at different culture times, static regulation strategies often lead to an imbalance of NADPH/NADP+ as they cannot adjust intracellular NADPH levels in real time [82].

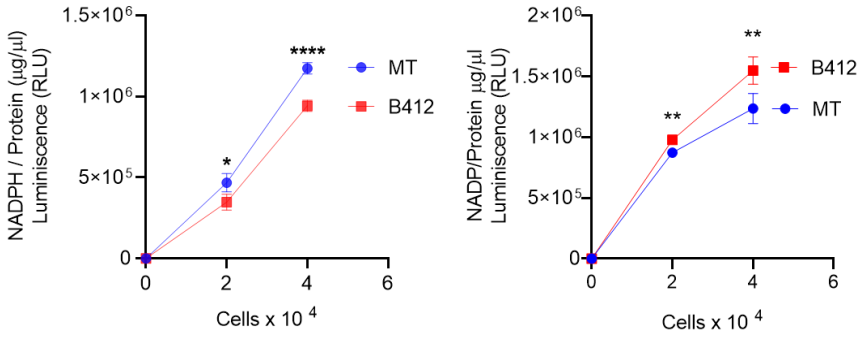

Figure 26. Analysis of NADPH production in MT and B412 cells 16 hours (left) and 6 hours (right) of $ZnSO_4$ treatment. Statistical analysis was performed by unpaired t-test by Welch's t-test: * $p \leq 0.05$, **$p \leq 0.005$, ***$p \leq 0.0005$.

4.6 Nuclear miR-223 enriches sequences located on metabolism-associated genes: Identification of SIRT1

The regulatory role of nuclear non-coding RNAs enhances the link between epigenetics and metabolism in leukemia. Binding of complementary sequences on DNA by miR-223 may participate in the epigenetic regulation of the expression of genes affecting different cellular processes. To identify the genomic regions bound by Cy5-labeled miR-223 and analyze their association with activating (H3K4me3) or repressive (H3K27me3) histone marks,

we performed ChIP-sequencing using specific antibodies in myeloid cells undergoing retinoic acid (RA)-induced granulocyte differentiation. Gene ontology (GO) analysis was conducted on genes whose transcription start sites (TSS) contained miR-223 complementary sequences enriched in the H3K4me3 mark, revealing several metabolism-related terms among the enriched categories (Fig. 27).

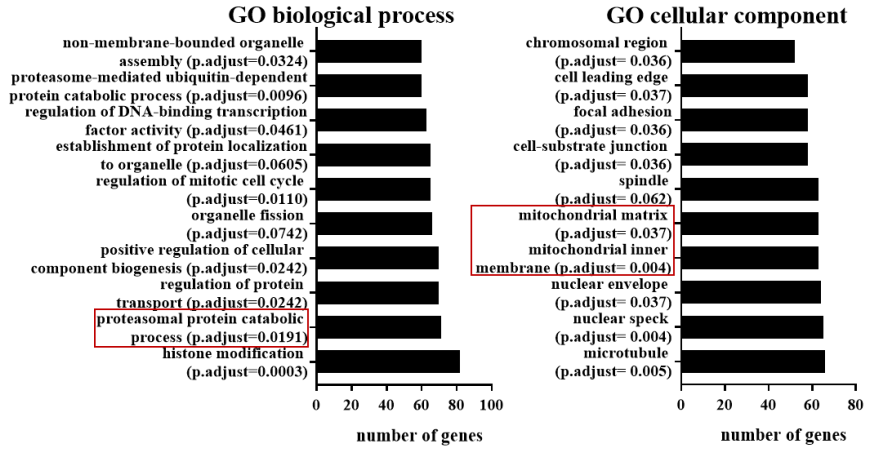

Figure 27. GO analysis of categories of genes bound by nuclear miR-223 at their TSS and enriched by H3K4me3 mark.

Based on these ChIP-seq data (Table 3), SIRT1 emerged as a potential nuclear target of miR-223, in a region associated with the activating H3K4me3 mark. SIRT1 is a central regulator of oxidative stress responses and metabolic adaptation.

Mitochondrial matrix	Mitochondrial Inner membrane	Proteasomal protein catabolic process
CARS2	LYN	HECTD3
PDHA1	OMA1	NFE2L2
PDPK1	OMA1	**SIRT1**
STYXL1	PARL	UBR2

Table 3. A list of nuclear targets of miR-223 identified by ChIP-seq

To further explore the relevance of miR-223 in this context, we measured its expression in patient-derived blasts. *miR-223* levels in PLZF::RARa-positive APL-like blasts (n = 4, 0.6 ± 0.3) were reduced compared to normal bone marrow (NBM; n = 3, 1.1 ± 0.5), PML::RARa-positive APL (n = 9, 0.9 ± 0.4), and AML samples (n = 7, 0.7 ± 0.5). Howewer, these differences were not statistically significant (Fig. 28A). Interestingly, induction of PLZF::RARa significantly reduced miR-223 levels compared to control cells (Fig. 28B).

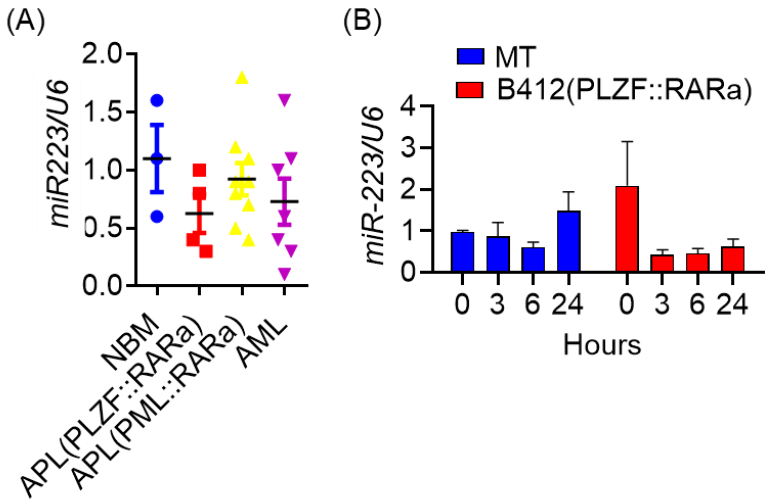

Figure 28. *miR-223* expression in Primary Hematopoietic cells. (A) Q-RT-PCR on miR-223 in 3 normal bone marrow (NBM), 4 PLZF::RARa+ APL-like, 9 PML::RARa-APL and 7 AML samples; (B) miR223 levels in a 24 h $ZnSO_4$ time course in B412 and MT control cells. Statistical analysis was performed using the Student's t-test.

Since the hematopoietic population is heterogeneous, achieving statistical significance is challenging; however, the observed trend, along with the results from the MT–B412 system, suggests that the metabolic alterations associated with the presence of the fusion protein may be linked to miR-223 expression and SIRT1 modulation. This connection could provide a mechanistic link between epigenetic regulation and cellular metabolic and antioxidant responses.

4.7 A Therapeutically Targetable SIRT1–FOXO3a Axis in PLZF::RARa+ cells

SIRT1 encodes a NAD^+-dependent deacetylase involved in the oxidative stress response and metabolic regulation, primarily through deacetylation of substrates such as FOXO3a. Analysis of

proteomic data from the Cancer Genome Atlas (TCGA) database indicated low SIRT1 protein levels across AML subtypes (Fig. 29A). Transcriptomic analysis by RNA-seq revealed significant downregulation of SIRT1 expression in all AML subtypes compared with healthy hematopoietic cell populations, although M3-AML samples displayed relatively higher levels (Fig. 29B).

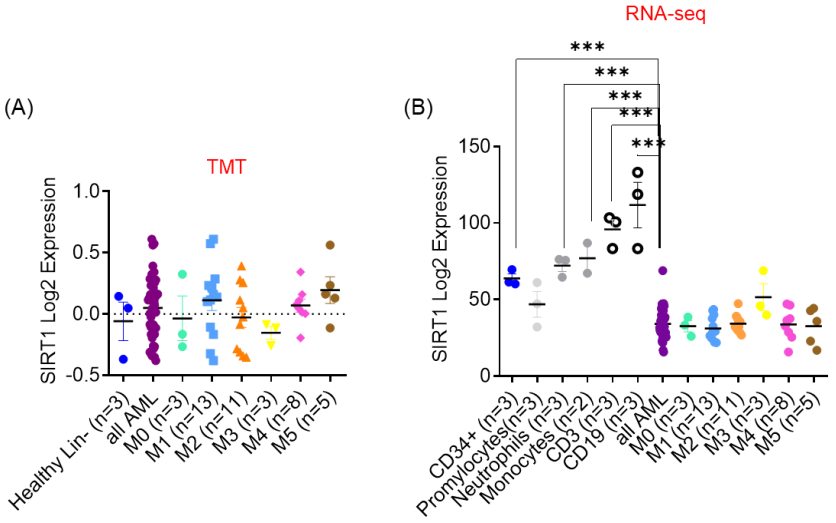

Figure 29. Proteomic (right) and Transcriptomic (left) profiling of SIRT1 Expression in Acute Myeloid Leukemia and Healthy Hematopoietic Controls.

These results are consistent with findings obtained in primary samples from our patients' cohort: *SIRT1* mRNA levels in PLZF::RARa+ APL-like patient blasts (n = 5, 1.7 ± 0.7) were comparable to those measured in normal bone marrow (NBM; n = 7, 1.2 ± 0.9) and in AML samples (n = 8, 1.2 ± 0.6). Overall, APL samples exhibited significantly higher *SIRT1* expression if compared to AML cases (p = 0.04) (Fig. 30).

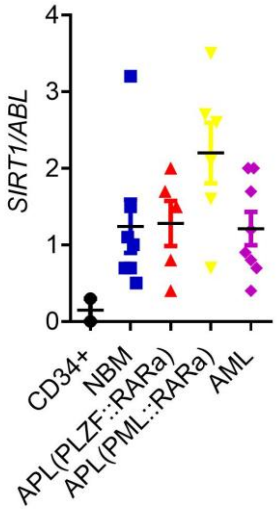

Figure 30. Functional validation of selected metabolic gene *SIRT1* in normal and neoplastic hematopoiesis. Q-RT-PCR on SIRT1 mRNA in 2 CD34+, 7 five normal bone marrow (NBM), 5 PLZF::RARa+ APL-like, 6 PML::RARa-APL and 6 AML samples. Statistical analysis was performed using unpaired t-test by Welch's t-test.

However, SIRT1 mRNA levels were significantly reduced upon PLZF::RARa induction compared to control cells (24 h: B412, 1.0 ± 0.3 vs MT, 1.9 ± 0.2; p = 0.01) (Fig. 31).

This downregulation was confirmed at the protein level (6 h: B412, 0.3 ± 0.1 vs MT, 0.5 ± 0.1; p = 0.03) (Fig. 32) suggesting that PLZF::RARa downmodulate SIRT1 expression.

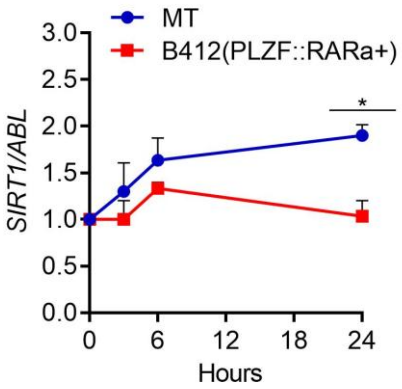

Figure 31. *SIRT1* mRNA expression induction in a 24 h time course after $ZnSO_4$ addition in B412 and MT control cells. The experiments were performed in triplicate. * p=0.01 by unpaired t-test by Welch's t-test.

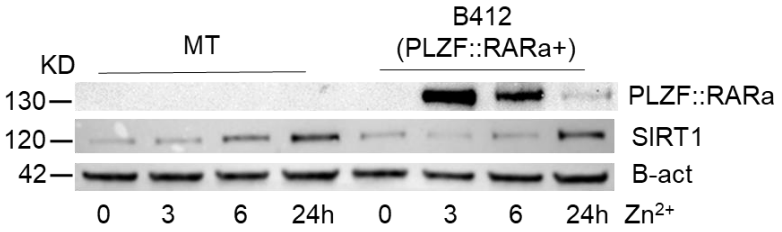

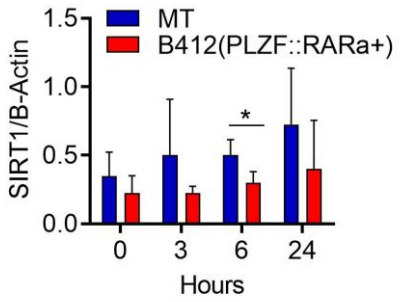

Figure 32. In B412 cells PLZF::RARa expression downregulates SIRT1 at the protein level. . The experiments were performed in quadruplicate. * p=0.03 by unpaired t-test by Welch's t-test.

The deregulated expression of SIRT1 was exacerbated by a direct interaction with PLZF::RARa. Imunofluorescence analysis revealed the nuclear colocalization of SIRT1 with PLZF::RARa in B412 cells was significantly higher than MT controls (Pearson's correlation coefficient: MT, 0.3 vs B412, 0.5; p = 0.006) (Fig. 33), suggesting that the fusion protein increases the recruitment of SIRT1 to the nucleus.

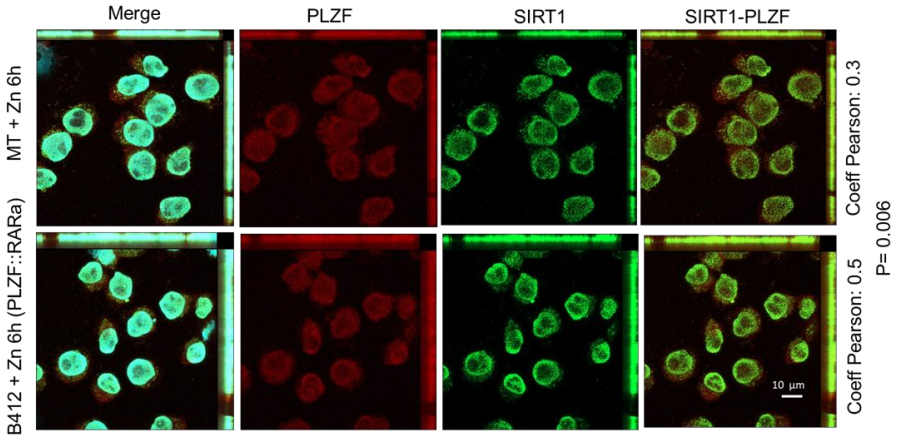

Figure 33. PLZF::RARa binds to SIRT1. Nuclear co-localization of PLZF::RARa and SIRT1 by confocal microscopy in PLZF::RARa+ B412 cells.

To directly assess the potential interactions between PLZF::RARa and SIRT1, we performed a proximity ligation assay (PLA) in control and PLZF::RARa-induced cells. Confocal microscopy revealed a marked increase in nuclear PLA signal in B412 cells 6 hours after $ZnSO_4$ induction, indicating that PLZF::RARa and SIRT1 are in a close molecular proximity, consistent with their physical interaction (Fig. 34).

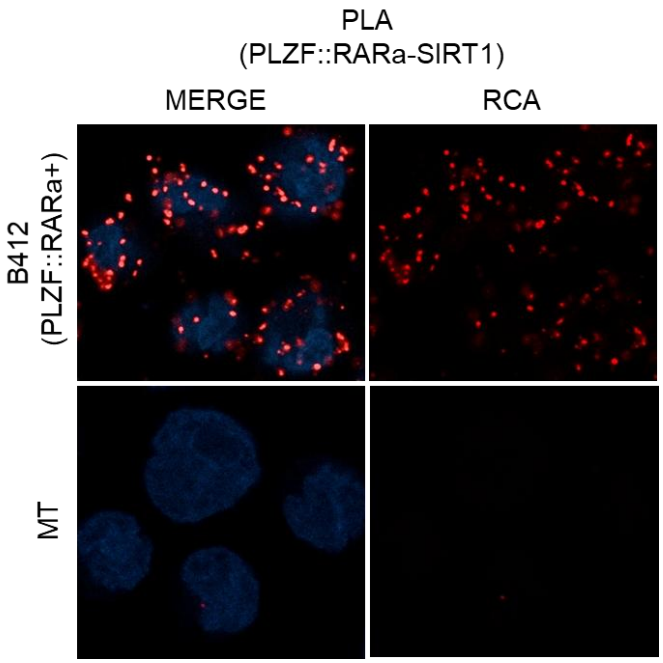

Figure 34. Detection of PLZF::RARa-SIRT1 protein interaction by proximity ligation assay (PLA) in B412 cells.

In PML::RARa expressing PR9 cells, PLA also generated a nuclear fluorescent signal, indicating that both these ÷RARα-fusion proteins can interact with SIRT1 within the nucleus (Fig. 35). These findings suggest that the association with SIRT1 is mediated through the RARa portion of the fusion protein. Such interactions may interfere with SIRT1 function.

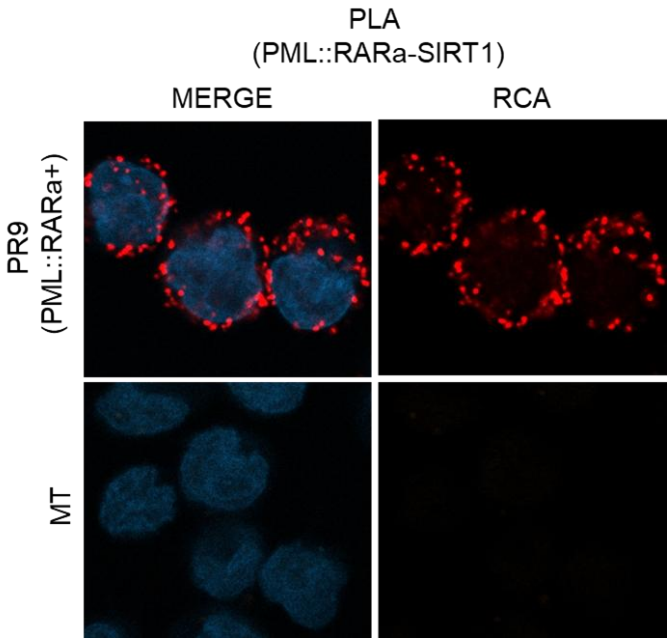

Figure 35. Detection of PML::RARa-SIRT1 interaction by PLA in PR9 cells.

4.8 PLZF::RARa impairs the activity of FOXO3a and its antioxidant targets via SIRT1-dependent deacetylation blockade

To investigate the functional consequences of the SIRT1–PLZF::RARa interaction and the observed reduction in SIRT1 activity, we analyzed the expression and activity of FOXO3a, a key transcription factor involved in antioxidant defense and a known SIRT1 substrate [83].
Proteomic and transcriptomic analyses using the Cancer Genome Atlas (TCGA) database revealed that FOXO3a expression is reduced in the M3-AML (APL) subtype compared to the other AML subtypes. While M0-, M1-, M2-AMLs, showed FOXO3a levels generally comparable among the AML group, M3- (APL), M4-, and

M5-AML samples were characterized by marked and consistent downregulation at both the mRNA and protein levels (Fig. 36A, Fig. 36B).

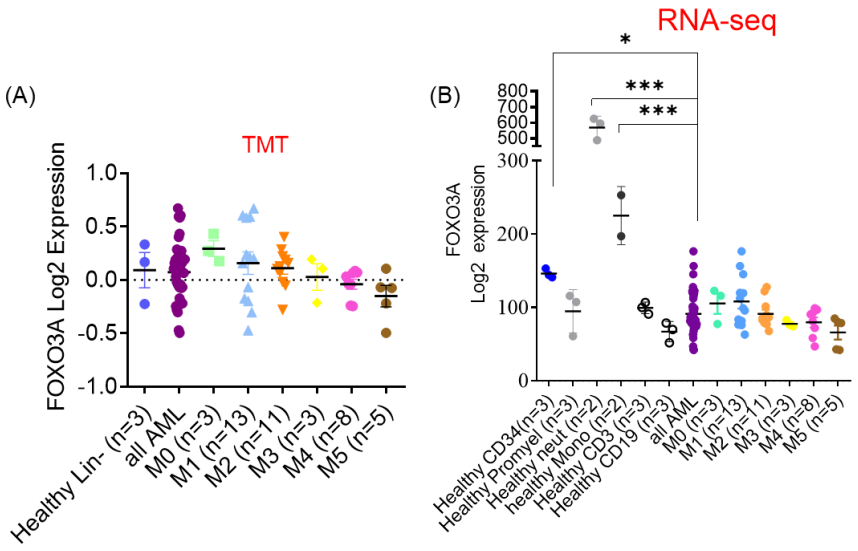

Figure 36. Proteomic (A) and Transcriptomic (B) profiling of FOXO3a expression in Acute Myeloid Leukemia and Healthy Hematopoietic Controls.

These findings corroborate our data showing a significant reduction in basal protein levels of FOXO3a in presence of the fusion protein PLZF::RARa compared with controls at 3h (MT| 1,3±0,3 vs B412| 0,7±0,2), at 6h (MT| 1,4±0,5 vs B412|0,5±0,3) and at 24h (MT| 1,9±0,4 vs B412|0,4±0,2) (p=0.01) (Fig. 37).

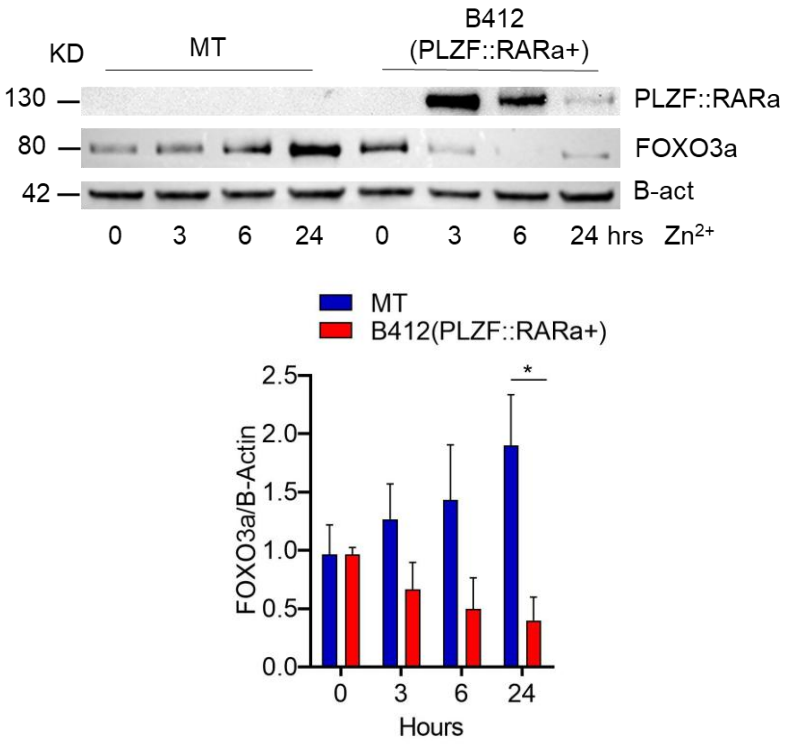

Figure 37. FOXO3a protein level increases and persists higher in a 24 h time course of $ZnSO_4$ treatment in MT control cells, whereas it decreases in PLZF::RARa+ B412 cells. The experiments were performed in triplicate. * p=0.01 by unpaired t-test by Welch's t-test.

In contrast, *FOXO3a* mRNA level was comparable between B412 and control cells over the 24-hour $ZnSO_4$ treatment (B412: 1,1 ± 0.1 vs. MT: 1.2 ± 0.4) (Fig. 38A), suggesting that FOXO3a may be regulated post-transcriptionally. FOXO3a mRNA levels were reduced in blasts from PLZF::RARa-positive APL-like patients (n = 4; 0.3 ± 0.1) and in PML::RARa-positive APL patients (n = 8; 0.4 ± 0.4) compared to AML blasts (n = 13; 0.3 ± 0.2) and NBM (n = 6; 1.9 ± 2.5), although the differences were not statistically significant (Fig. 38B).

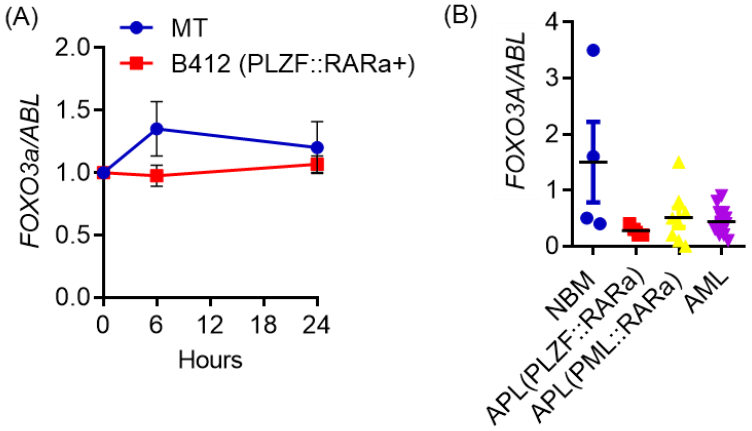

Figure 38. *FOXO3a* mRNA expression in Cell lines and Primary Hematopoietic cells. (A) FOXO3a mRNA expression in a 24 h time course after $ZnSO_4$ addition in B412 and MT cells. The experiments were performed in quadruplicate. (B) Q-RT-PCR analysis of FOXO3a mRNA levels in 5 NBM and in patient-derived blasts: 4 PLZF::RARa-positive APL like, 8 PML::RARa-positive APL and 13 AML samples. Statistical analysis was performed by unpaired t-test by Welch's t-test.

SIRT1 deacetylates and activates FOXO3a, promoting the transcription of antioxidant genes [60]. The reduction in SIRT1 expression observed in PLZF::RARa+ B412 cells is expected to compromise the deacetylation and function of FOXO3a. Co-immunoprecipitation experiments perfomed using an anti-pan-acetyl-lysine antibody revealed that PLZF::RARa expression interferes with FOXO3a deacetylation, likely due to reduced SIRT1 expression, leading to the accumulation of its acetylated, transcriptionally inactive, form (Fig. 39).

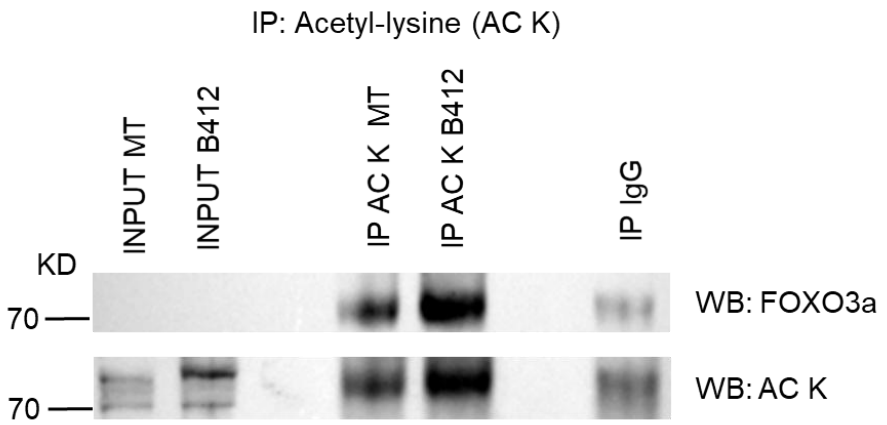

Figure 39. Enhanced acetylation of FOXO3a in B412 cells.

As a consequence, B412 cells displayed a reduced transcription of downstream FOXO3a target genes involved in antioxidant defense, including *SOD1* (6 h: MT, 1.6 ± 1 vs. B412, 0,7± 0,3) (Fig. 40A) and *Catalase* (6 h: MT, 1.5 ± 0.9 vs. B412, 0,8 ± 0.2) (Fig. 40B).
In patient samples: *SOD1* mRNA in PLZF::RARa-positive APL-like blasts was reduced significantly (n = 4, 0.3 ± 0.3) (p=0.04) if compared to PML::RARa-positive APL (n = 8, 1.7 ± 1.8); but not if compared to normal bone marrow (NBM, n = 6, 1.3 ± 1.1), or AML samples (n = 13, 0.7 ± 1) (Fig.40C). *Catalase* mRNA expression in PLZF::RARa+ APL-like patient blasts (n = 4, 1.4 ± 0.9) was similar to that of normal bone marrow cells (NBM, n = 6, 1.8 ± 1.2) and AMLs (n = 13, 0.7 ± 0.5). However, it was reduced if compared to PML::RARa-positive APL (n = 8, 1.8 ± 1.8) (Fig. 40D).

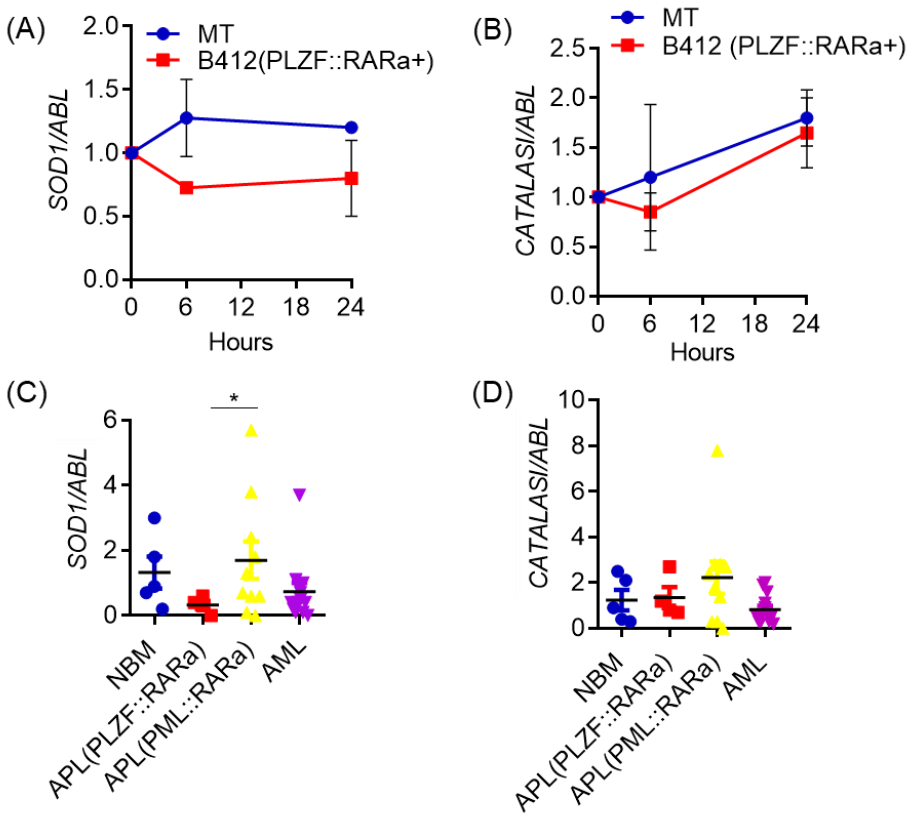

Figure 40. mRNA expression of FOXO3a target genes in cell lines and primary hematopoietic cells**.** mRNA expression of *SOD1* (A) and (B) *Catalase* over 24 hours following $ZnSO_4$ treatment in MT and PLZF::RARa+ B412 cells. The experiments were performed in quadruplicate. Statistical analysis was conducted by unpaired t-test by Welch's t-test (C) Q-RT-PCR on *SOD1* mRNA in 5 NBM, 4 PLZF::RARa+ APL-like, 10 PML::RARa-APL and 13 AML samples; (D) Q-RT-PCR on *Catalase* mRNA in NBM (n=5), 4 PLZF::RARa+ APL-like (n=4), PML::RARa-APL (n=10) and AML (n=13) samples. * p=0.04 by unpaired t-test by Welch's t-test

Functionally, FOXO3a inactivation resulted in impaired antioxidant defenses. SOD1 protein levels were significantly decreased after 3h $ZnSO_4$ induction in B412 (MT: 0.52 ± 0.01 vs. B412: 0.23 ± 0.1; p

= 0.008) (p=0.04) and remained lower at 6 h (MT: 0.86 ± 0.28 vs. B412: 0.49 ± 0.08) (p=0.05) (Fig.41).

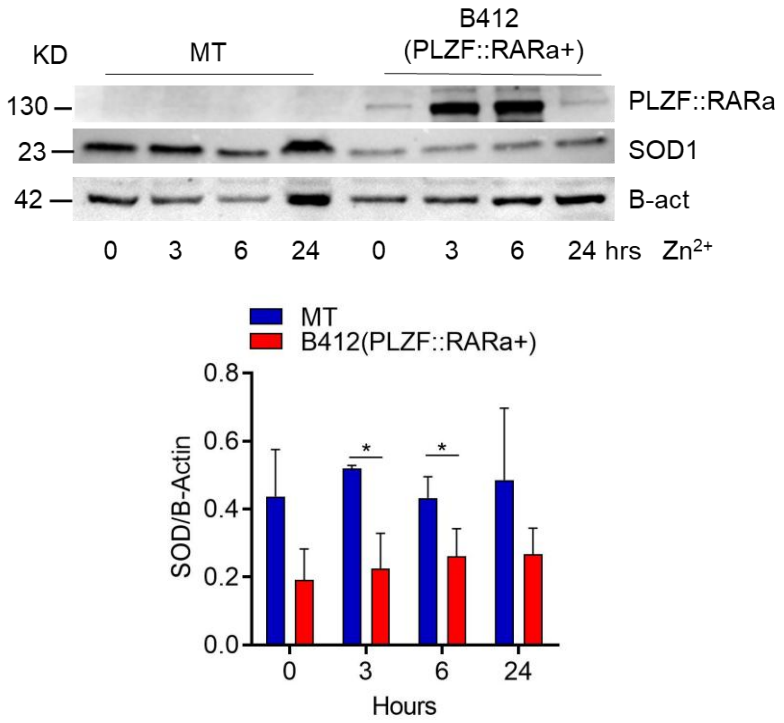

Figure 41. Decreased SOD1 protein expression in presence of PLZF::RARa in B412 cells. The experiments were performed in triplicate. * p =0.05 by unpaired t-test by Welch's t-test.

Catalase enzymatic activity, expressed as Units per milliliter (U/mL), was reduced in B412 cells (MT: 2,71 ± 0,10 vs B412: 1,16 ± 0,92; ≈ 57 % reduction) (Fig. 42).

Altogether, these findings provide evidence that the interaction of PLZF::RARa with SIRT1 promotes redox imbalance by impairing SIRT1-dependent deacetylation of FOXO3a, which in turn results in reduced SOD1 protein expression and decreased catalase enzymatic activity. Overall, these alterations compromise several levels of the redox protection mechanism in PLZF::RARa-positive

cells, making them more sensitive to pro-oxidant treatments and highlighting oxidative stress as a potential therapeutic vulnerability in this subtype of leukemia.

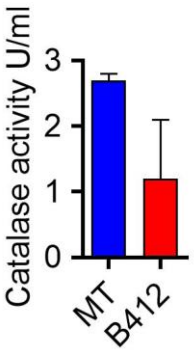

Figure 42. Reduced catalase activity in presence of PLZF::RARa fusion protein in B412 cells. Data are shown as mean ± SD from two independent experiments.

4.9 PLZF::RARa+ Cells Exhibit Sensitivity to Ascorbate Treatment and Mitochondrial Dysfunction in Response to Combination Therapies

To further explore these mechanistic vulnerabilities, we evaluated several pro-oxidant-based treatments. Since ASC treatment has shown efficacy in APL samples [64], we investigated its potential interference with the disease-specific PLZF::RARa oncoprotein. To this end, we treated primary blasts from a PLZF::RARa+ patient with increasing concentrations of ASC (1 and 3 mM) and/or arsenic trioxide (ATO, 1 μM) for 72 hours. Apoptosis was assessed by flow cytometry using Annexin V/ /Live-Dead assay. ASC induced apoptosis in a dose-dependent manner, with 47% apoptosis at ASC 1 mM and 99% at 3 mM, compared to 14% in untreated cells. ATO (1 μM) alone induced apoptosis (46%), while in combination with ASC (3 mM) the apoptotic cells were 86.3% (Fig. 43).

To further evaluate the efficacy of ASC in the treatment of PLZF::RARa+ APL-like disease, we analyzed mitochondrial

membrane potential (ΔΨm) as a marker of apoptosis in B412 and MT control cells. Cells were treated with ASC (1 mM), AZA (100 ng/mL), or their combination for 48 hours, followed by staining with JC-1 dye.
Increased apoptosis was observed in B412 cells treated with AZA (24%), ASC (42%) and the combination (63% apoptosis) (Fig. 44 top), compared to control cells (ASC: 12%; ASC+AZA: 30% apoptosis) (Fig. 44 down).

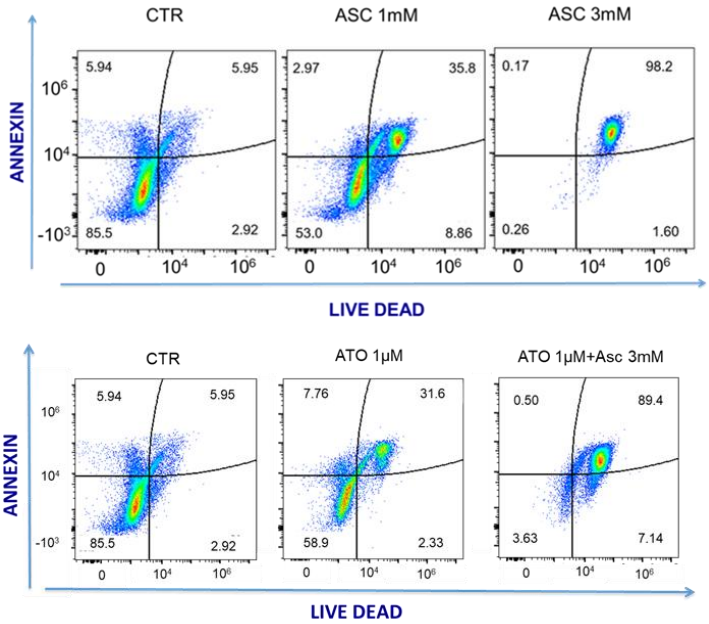

Figure 43. Apoptosis in APL PLZF::RARa primary blast cells treated with Ascorbate (ASC1 and 3 mM) and arsenic trioxide (ATO, 1 µM) for two days.

Consistent with JC-1 data (ΔΨm), immunoblot analysis revealed activation of the cleaved Caspase-3 (Fig. 45 top) and PARP1 (Fig. 45 down)—key markers of apoptosis—after 48 hours of treatment with ASC or AZA in PLZF::RARa+ B412 cells. These cleaved forms were markedly increased following the combined ASC-AZA treatment, indicating a synergistic activation of apoptotic pathways.

In contrast, MT control cells exhibited faint cleavage of these proteins across all treatment conditions, underscoring the selective vulnerability of PLZF::RARa-expressing cells to redox-based and epigenetic therapies.

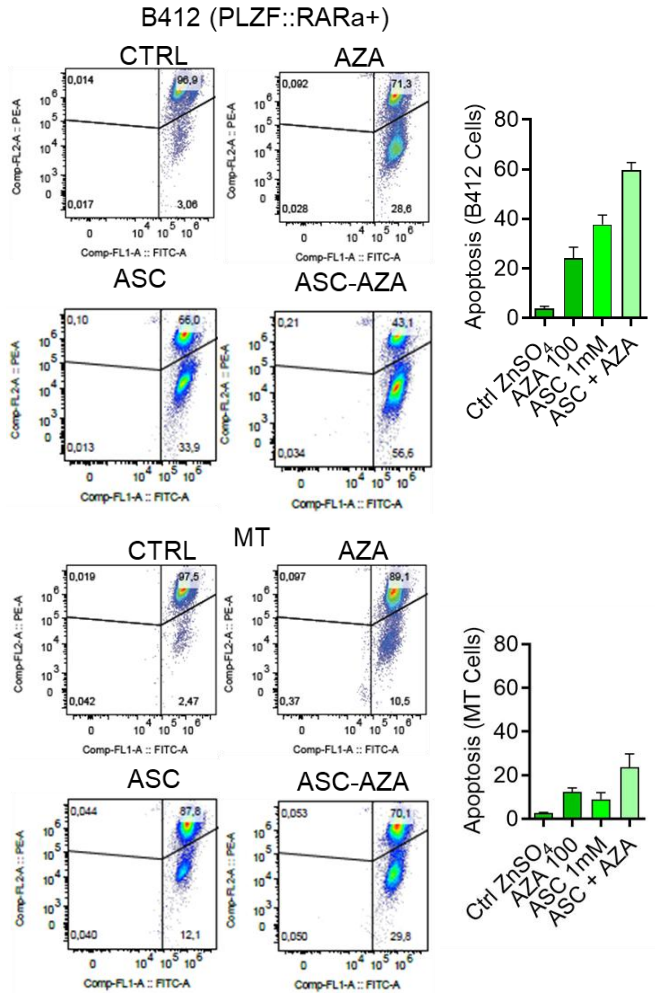

Figure 44. Apoptosis Analysis by JC-1, measuring mitochondrial membrane potential (ΔΨm) (Flow Cytometry) in B412 (PLZF::RARa+) and MT (ctrl) cells untreated and treated with AZA and ASC for 48 hours. The experiment was performed in duplicate.

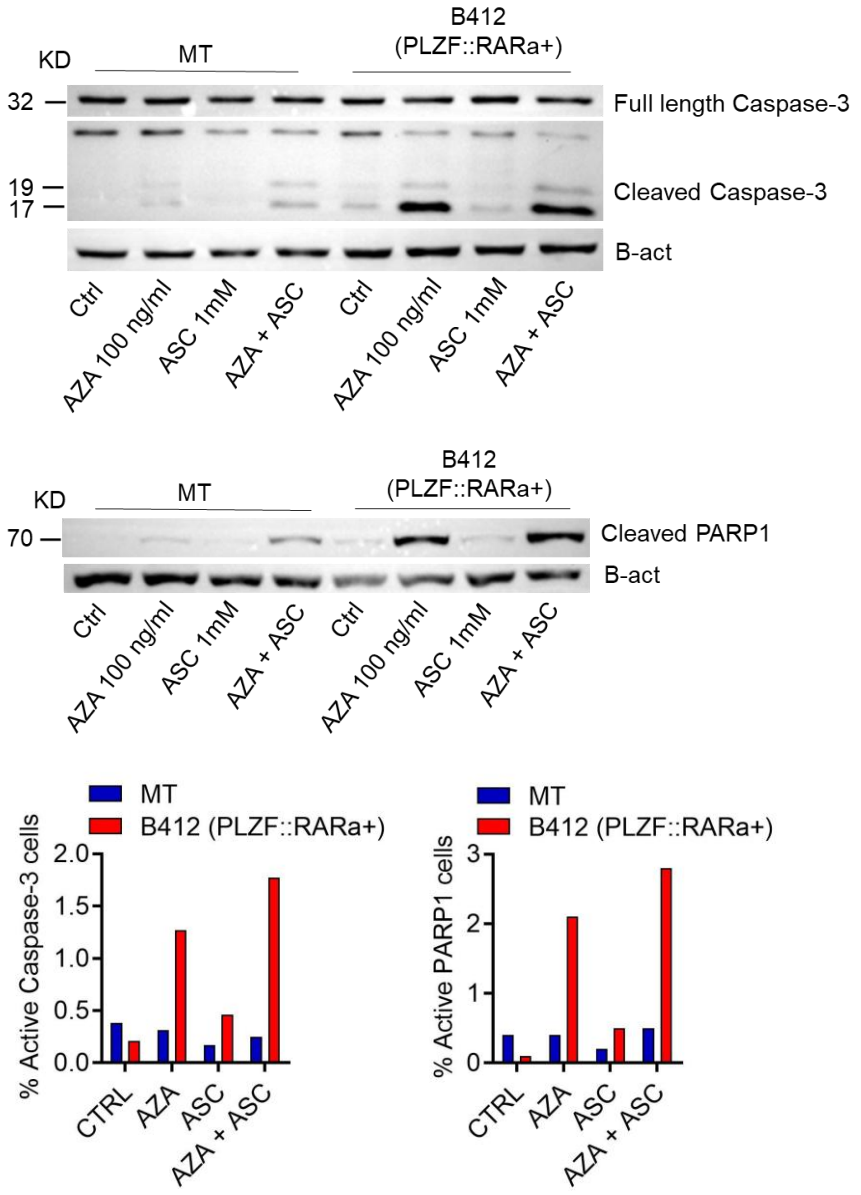

Figure 45. Western blot analysis of apoptotic markers in MT and B412 cells. Detection of cleaved caspase-3 (up) and cleaved PARP-1 (down) proteins as indicators of apoptosis. β-actin was included as a loading control.

These data indicate that PLZF::RARa-expressing cells are more susceptible to oxidative stress and mitochondrial injury, and that ASC, particularly in combination with AZA, enhances apoptotic cell death.

4.10 Synergistic Activity of Venetoclax and Azacitidine (VEN + AZA) in PLZF::RARa+ cells

Aberrant overexpression of BCL-2 family proteins contributes to chemotherapy resistance. The combination of Venetoclax (VEN), a selective BCL2 inhibitor, and Azacitidine (AZA), which indirectly targets MCL1 and BCL-XL, is currently the standard of care for patients with newly diagnosed AML who are unfit for intensive chemotherapy. Given the metabolic rewiring characterized by high OXPHOS, associated with PLZF::RARa mutation, and the ability of VEN to disrupt mitochondrial function and interfere with the cellular oxidoreductive system, this combination may represent a promising therapeutic strategy for APL-like PLZF::RARa patients resistant to ATO and ATRA therapy. To evaluate the potential efficacy of this therapeutic combination in PLZF::RARa-positive leukemia, B412 cells and MT control cells were treated with VEN (10 nM), AZA (100 ng/mL), alone or in combination for 48 hours. Apoptosis analysis by JC-1 dye, assessing mitochondrial membrane potential (ΔΨm), showed that the VEN-AZA combination caused a marked reduction in ΔΨm in B412 cells (AZA: 24%; VEN: 8%; AZA+VEN: 31% apoptosis) (Fig. 46 top) compared to MT controls (AZA: 12%; VEN: 4%; AZA+VEN: 14% apoptosis) (Fig. 46 down), indicating mitochondrial depolarization and apoptosis inductions.

Immunoblot analysis further confirmed the activation of apoptotic signaling, as evidenced by the cleavage of caspase-3and PARP-1 in B412 cells treated with either agent alone, with a more pronounced effect following VEN–AZA co-treatment. In contrast, only faint levels of cleaved caspase-3 and PARP-1 were detected in MT control cells. (Fig. 47).

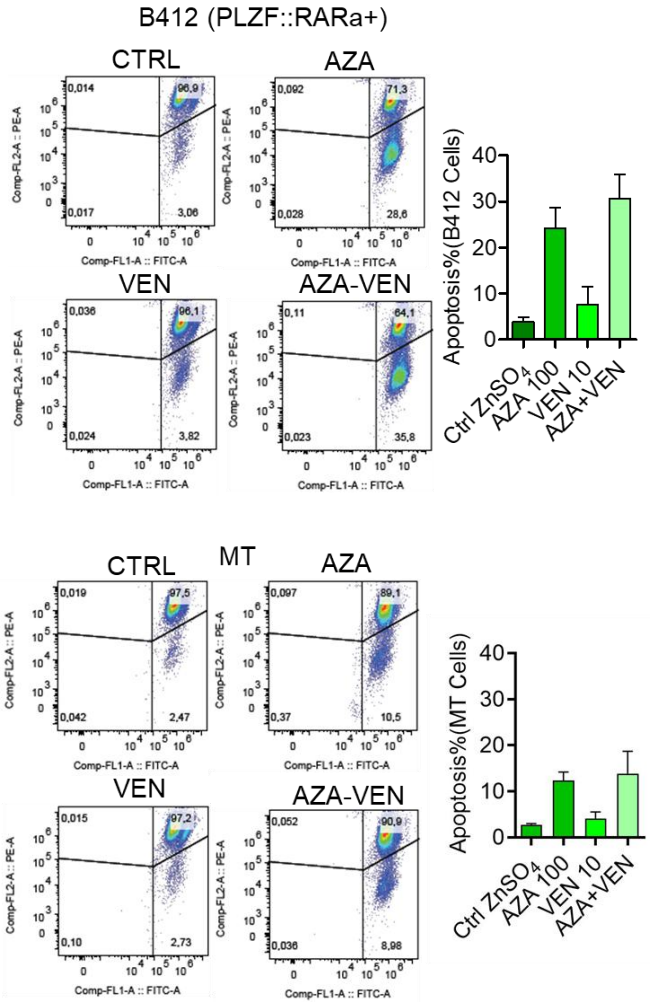

Figure 46. Apoptosis Analysis by JC-1, measuring mitochondrial membrane potential (ΔΨm) (Flow Cytometry) in B412 (PLZF::RARa+) and MT (ctrl) cells untreated and treated with AZA and VEN for 48 hours. The experiment was performed in duplicate.

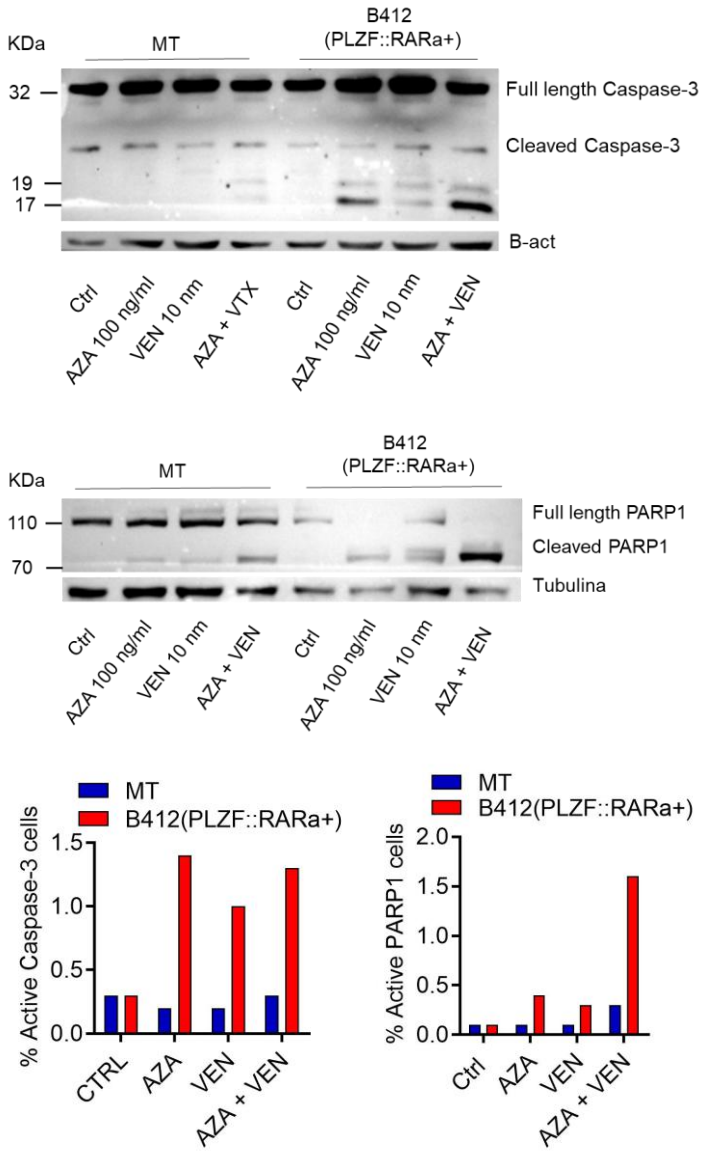

Figure 47. Western blot analysis of apoptotic markers in MT and PLZF::RARa+ B412 cells. Detection of cleaved caspase-3 (up) and cleaved PARP-1 (down) proteins as indicators of apoptosis, in MT and B412 cells. β-actin was included as a loading control.

Building on these findings, we next sought to determine whether the combination of VEN and AZA exerted synergistic rather than merely additive effects. Consistently, cell viability assays (MTT) demonstrated a synergistic inhibitory impact of VEN–AZA on B412 cell proliferation (ZIP synergy score: 11.0; MSA: 21.69), whereas the effect was less pronounced in MT cells (ZIP: 5.77; MSA: 10.77). (Fig. 48).

Epigenetic inhibitors such as AZA or decitabine can alter chromatin structure and modulate the transcription of genes regulated by PLZF::RARa [84], supporting the hypothesis that interference with PLZF::RARa signaling sensitizes these cells to oxidative stress and mitochondrial damage.
These findings suggest that PLZF::RARa+ cells are particularly vulnerable to mitochondrial apoptosis induced by the VEN-AZA combination, and suggest that integrating agents targeting PLZF::RARa function or antioxidant defenses with redox-based therapies may represent a promising approach to overcome treatment resistance in this aggressive leukemia subtype.

	Drug combination	Synegy score	Most synergistic area score	Method
B412	VEN-AZA	11	21.69	ZIP
MT	VEN-AZA	5.77	10.77	ZIP

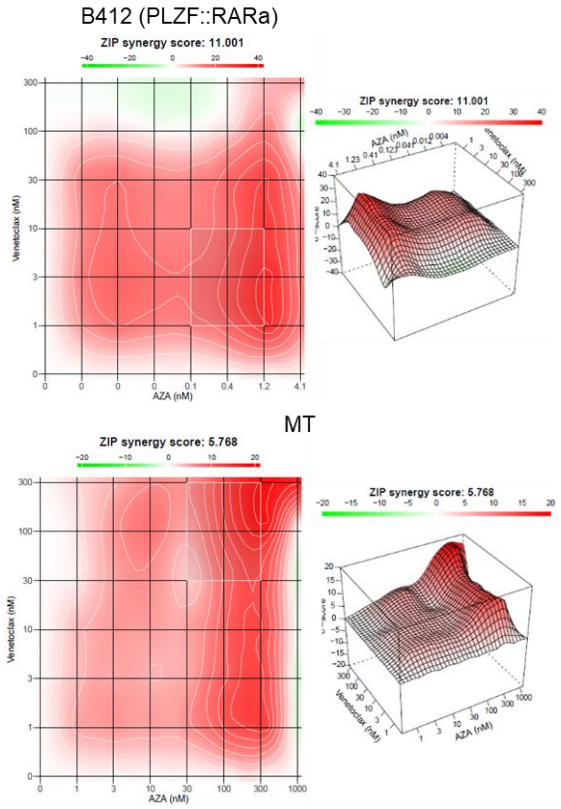

Figure 48. Synergistic activity of venetoclax and azacytidin on B412 and MT. Two dimension (2D) and 3D synergy map for the combination of VTX (0 to 300 nM) and AZA (0 to 1000 ng/ml) analyzing cell grow by MTT assay. The data represent three independent biological replicates performed in MT and B412 (PLZF::RARa+) cells The ZIP score (∂-score) for each drug combination is indicated by the color code given above the panel grid (synergistic and antagonistic dose regions in red and green colors, respectively). ZIP score >10 indicates synergism; ZIP score between -10 and 10 indicates additivity; and ZIP score <-10 indicates antagonism.

5. DISCUSSION

Acute myeloid leukemias (AMLs) are aggressive hematologic malignancies characterized by blocked differentiation, uncontrolled proliferation, and poor clinical outcomes, particularly in the elderly. Among AMLs, t(11;17)-APL-like subtypes expressing the PLZF::RARa fusion protein differ from classical t(15;17)-APLs (expressing PML::RARa) due to their resistance to ATRA- and ATO-based therapies, which have dramatically improved outcomes for t(15;17)-APL patients [85]. PLZF::RARa is known to act as a potent transcriptional repressor by recruiting co-repressor complexes, histone deacetylases, and chromatin remodeling factors to its target genes. This function suggests that it may interfere with metabolic and redox pathways. Beyond genetic and epigenetic alterations, AML cells are sustained by profound metabolic rewiring [86]. While cancer cells are generally known for their high glycolytic activity [40], our data indicate that PLZF::RARa-positive APL-like blasts rely primarily on mitochondrial oxidative phosphorylation (OXPHOS) and fatty acid oxidation to meet their energetic and biosynthetic demands. Glycolysis remains active but appears slightly reduced compared with control cells, indicating a shift toward mitochondrial metabolism rather than a classic Warburg-like phenotype.

We characterized the metabolic profile of AML blasts compared to normal hematopoietic progenitors and precursors. Leukemic blasts exhibited increased mitochondrial activity but reduced respiratory reserve capacity compared with normal counterparts, suggesting heightened susceptibility to oxidative stress [39]. Metabolism plays a defining role in APL biology. Work on the classic PML::RARa that causes APL has shown that the fusion protein profoundly alters the metabolic landscape. PML::RARa reduces glycolytic dependence by promoting AKT degradation, thereby limiting pyruvate availability and glycolytic flux. Despite the presence of glycolytic enzymes, APL cells are unable to utilize glycolysis

efficiently and compensate by increasing mitochondrial respiration, which is primarily fueled by the oxidation of long-chain fatty acids. This metabolic configuration distinguishes APL from normal promyelocytes, which maintain a strong glycolytic dependence, and from other subtypes of AML[86].

Focusing on the PLZF::RARa-positive APL-like subtype, we observed that both primary blasts and B412 cells, induced to express PLZF::RARa by $ZnSO_4$ treatment, displayed enhanced mitochondrial respiration relative to normal progenitors. This increased mitochondrial activity is typically associated with elevated electron transport chain flux, which can lead to higher electron leakage and, consequently, augmented production of reactive oxygen species (ROS) [81]. Based on these findings, we investigated the role of PLZF::RARa in modulating the cellular defense against oxidative stress.

Our data indicate that PLZF::RARa expression profoundly disrupts the cellular antioxidant defense network at multiple levels.

Normal hematopoietic cells rely on NRF2 to coordinate the adaptive antioxidant response. Its relevance in myeloid transformation is supported by data from classical t(15;17)-APL: Banella et al. demonstrated that PML::RARa modulates NRF2 signaling, inhibiting its transcriptional activity and altering antioxidant responses. These findings underscore that NRF2 dysregulation is a key feature of APL biology[56].

In normal hematopoietic cells, the NRF2 pathway regulates the adaptive antioxidant response by activating genes involved in detoxification (HO-1), glutathione synthesis control, and the pentose phosphate pathway (PPP). The PPP, through the activity of G6PDH, is the main source of cytosolic NADPH, which supports ROS neutralization. AML cells with high oxidative stress become increasingly dependent on NRF2-driven pathways to maintain viability, and disruption of this axis increases their sensitivity to metabolic stress.

PLZF::RARa-positive cells exhibited a significant elevation of intracellular ROS, which correlated with impaired NRF2 signaling.

Since NRF2 is a master regulator of the adaptive response to oxidative stress, its deregulation led to defective induction of downstream target gene HO-1, compromising the ability of leukemic cells to cope with oxidative insults. This vulnerability was further reinforced by a marked reduction in G6PDH expression and NADPH availability, impairing ROS detoxification; given that G6PDH is a direct transcriptional target of NRF2 [54], this finding underscores the disruption of NRF2-dependent metabolic regulation.
The SIRT1-FOXO3a axis acts as a central regulator of redox homeostasis and metabolic adaptation in hematopoietic cells. SIRT1, an NAD^+-dependent deacetylase, regulates metabolic and oxidative signals by modulating the activity of several transcription factors, including FOXO3a. SIRT1 promotes the expression of antioxidant genes, including MnSOD and catalase, through FOXO3, supporting the idea that SIRT1-FOXO3a signaling is a key component of the adaptive response to oxidative stress[87].

When deacetylated by SIRT1, FOXO3a becomes transcriptionally active and promotes the expression of key antioxidant and cytoprotective genes, including SOD1, catalase, and genes involved in the response to DNA damage. This regulatory network ensures that hematopoietic stem and progenitor cells maintain quiescence and preserve mitochondrial integrity. In AML, this balance is often compromised. Leukemic cells often have elevated levels of mitochondrial ROS due to increased OXPHOS activity and modulate SIRT1 and FOXO3a to mitigate oxidative stress. Leukemias characterized by epigenetic dysregulation or altered transcriptional activity often exhibit impaired SIRT1 activity, leading to persistent acetylation of FOXO3a and loss of its transcriptional program. Acetylated FOXO3a becomes unstable and transcriptionally inactive, resulting in decreased expression of antioxidant genes and increased susceptibility to oxidative damage.
Our results show that the reduction of SIRT1 expression was exacerbated by a direct interaction with PLZF::RARa, which likely

further alters its function. As a consequence, FOXO3a becomes hyperacetylated and inactivated, leading to reduced expression of essential ROS scavengers, including SOD1 and catalase, which adds to defects in the NRF2 pathway and further compromises the antioxidant capacity of PLZF::RARa-positive cells. These results extend the concept that the oncogenic fusion protein remodel stress-response networks at multiple levels, including SIRT1–FOXO3a-dependent antioxidant control. In combination with the increased OXPHOS dependence and NRF2 dysfunction observed in our models, the impairment of SIRT1–FOXO3a–SOD1/catalase signaling delineates a redox-vulnerable phenotype.
Collectively, these alterations compromise multiple layers of the redox-protective machinery in PLZF::RARa-positive cells, functionally rendering them more susceptible to pro-oxidant treatments and highlighting oxidative stress as a potential therapeutic vulnerability in this leukemia subtype.
The interplay between epigenetic and metabolic regulation is a central feature of myeloid differentiation. MicroRNAs regulate a variety of biological processes, from cell fate and proliferation to differentiation and apoptosis. The regulatory role of nuclear non-coding RNAs enhances the link between epigenetics and metabolism in leukemia. ChIP-seq data identified miR-223-bound genomic regions associated with histone marker activation, including metabolic gene promoters. miR-223 emerges as a key regulatory molecule for chromatin status and metabolic programming and contributes to the regulation of myeloid differentiation. Given the critical role of miR-223 in granulopoiesis, its involvement in metabolic regulation adds an additional layer of control that may converge on targets such as SIRT1. These observations suggest that miR-223 may represent an epigenetic modulator linking chromatin regulation to metabolic adaptation in myeloid differentiation.

In line with these mechanistic vulnerabilities, we tested several pro-oxidant-based therapies. Ascorbate exhibits distinct biological

activities depending on its concentration. At physiological levels, it can enhance the action of hypomethylating agents (HMAs) by facilitating DNA demethylation, thereby promoting the apoptosis of malignant cells. When administered at pharmacological doses, ascorbate acts as a pro-oxidant role. In AML models, high-dose ascorbate intensifies oxidative stress and promotes ROS accumulation, ultimately inducing apoptosis of leukemic cells. This pro-oxidant activity shows marked cytotoxic effects in vitro, in combination with Azacitidine (AZA). Treatment with high-dose ascorbic acid significantly reduced cell viability, an effect that was further potentiated by combination with AZA. AZA-VEN combination exploits the metabolic vulnerability of AML cells with increased mitochondrial dependence. VEN, a selective BCL2 inhibitor, compromises mitochondrial integrity by promoting apoptosis; its efficacy is greatly enhanced in AML subgroups that depend on OXPHOS for survival. AZA complements this mechanism through epigenetic reprogramming: altering chromatin accessibility and modulating transcriptional programs. The combination of VEN with AZA was also highly effective in PLZF::RARa-positive cells, inducing profound mitochondrial depolarization and strong caspase activation. Importantly, epigenetic inhibitors such as AZA or decitabine can alter chromatin and modulate the expression of genes regulated by PLZF::RARa [84], further supporting the concept that interfering with PLZF::RARa signaling can sensitize these cells to oxidative stress. Overall, our results suggest that integrating agents that disrupt PLZF::RARa function or antioxidant defences with redox-based therapies may represent a promising approach to overcome treatment resistance in this aggressive leukemia subtype.

In conclusion, our findings provide a mechanistic framework linking PLZF::RARa to metabolic and redox regulation, offering new avenues for targeted therapies in refractory APL-like.

6. MATHERIALS AND METHODS

6.1 Primary Patients' Samples

Bone marrow (BM) samples were collected from patients diagnosed with de novo AML admitted at the Department of Hematology of the University of Rome Tor Vergata. All samples had at least 70% infiltration by leukemic blasts. Written informed consent was obtained from all patients in accordance with the Declaration of Helsinki and the study was approved by the ethical committee of the University of Rome Tor Vergata.

The separation of mononuclear cells (blasts, lymphocytes, monocytes) from whole bone marrow blood samples and peripheral blood was performed by density gradient centrifugation using Ficoll/Hypaque (Lympholyte® - Caderlane), a solution based on polysaccharose and sodium diatrizoate. This method allows the separation of cellular and acellular components contained in the blood. In particular, polysaccharose promotes the aggregation of erythrocytes and granulocytes and their subsequent rapid sedimentation. Lymphocytes, monocytes, and blasts are retained at the interface between the Lympholyte® solution and the plasma to form an opalescent ring of cells. The sample was diluted with an appropriate volume of sterile physiological solution (1:2 bone marrow blood, 1:3 peripheral blood) at room temperature. The diluted blood was slowly layered into a test tube containing 3.5 ml of Ficoll for every 5 ml of diluted sample, using a sterile disposable Pasteur pipette. The sample was centrifuged at 2200 rpm for 20 minutes, and then the ring of mononuclear cells, formed at the interface between the plasma (upper phase) and the Ficoll (lower phase), was removed using a sterile pipette. The separated cells, washed in physiological solution, were counted and resuspended partially in Trizol (Life Technologies, Invitrogen, USA) and partially pelleted and stored at minus 80°C. The cells stored in Trizol were subsequently used for total RNA extraction, while the others were used for protein fraction extraction.

6.2 *Cell lines and cell culture*

U937-MT (a monoblastic cell line constructed with the empty vector from the U937 cell line) used as control and U937-B412 (a zinc-inducible PLZF::RARa model constructed from the U937 cell line) were kindly provided by by Prof. Estelle Duprez from the Marseille Cancer Research Center (CRCM), Aix-Marseille University, France.The cells were cultured in RPMI medium (Euroclone; Pero, MI, Italy) 10% fetal bovine serum (FBS) (GIBCO-BRL) 20 mM Hepes, 100 U/mL penicillin and 100 µg/mL streptomycin (GIBCO-BRL). Cultures were maintained at 37°C in a 5% CO2 humidified incubator.

6.3 Western blotting and co-immunoprecipitation

Protein samples were separated by SDS–polyacrylamide gel electrophoresis and transferred to nitrocellulose membranes (Perkin Elmer, Cat# NBA085B). Membranes were blocked for 1 h in Tris-buffered saline solution with 0.1% Tween-20 (TBS-T) containing 5% BSA and then incubated overnight at 4°C with indicated primary antibodies, diluted in TBS-T containing 3% BSA.
After rinsing with PBS-T solution, membranes were incubated for 1 h with the appropriate peroxidase-conjugated secondary antibody diluted in 3% of Milk. Then washed and developed using the enhanced chemiluminescence detection system (BIO-RAD ClarityTM Western ECL substrate Cat# 170- 5061). Densitometric analyses were performed using ImageJ software program (U. S. National Institutes of Health, Bethesda, Maryland, USA, https://imagej.nih.gov/ij/, 1997-2016). The primary antibodies used are reported in Table 4. For co-immunoprecipitation assays, protein extracts (2–4 mg) were incubated at 4 °C overnight with 2 µg of anti-PLZF, anti-NRF2 and anti Acetyl Lysine antibodies conjugated with Protein G–Dyna beads (Invitrogen, Oslo, Norway). Immunoprecipitated protein complexes were resolved on SDS polyacrylamide gels followed by western blot.

Antibody	Source	Identifier
Acetyl Lysine	Cell Signaling, Danvers, MA, USA	# 9441
β-ACTIN	Sigma , Deutschland, GmbH	# 3700
Caspase 3	Cell Signaling, Danvers, MA, USA	# 14220
FOXO3a	Cell Signaling, Danvers, MA, USA	# 12829
G6PDH	Cell Signaling, Danvers, MA, USA	# 12263
HO-1	Cell Signaling, Danvers, MA, USA	# 5853
IgG Rabbit	Cell Signaling Inc (MA, USA)	# 2729S
NRF2	Proteintech	# 16396-1-AP
Cleaved-PARP	Cell Signaling, Danvers, MA, USA	# 32563
PARP1	Abnova	# H00000142-M01
PLZF	Santa Cruz Biotechnology, INC	#sc-28319
PLZF	Cell Signaling, Danvers, MA, USA	# 39784
SIRT1	Novus	# NBP1-51641
SOD1	Cell Signaling, Danvers, MA, USA	# 4266

Table 4. List of Primary Antibodies

6.4 Analysis of mRNA Expression by Real-Time PCR

Total RNA was extracted with Trizol, and reverse transcription was performed with 1 μg of total RNA following a standardized protocol (Applied Biosystems, Foster City, CA, USA). mRNA expression levels were determined by Real Time qPCR reactions by Light Cycler 480 SYBR Green System (Roche ETC) following manufacturer indications. Cp values were calculated using the 'second derivative max' algorithm of the Lightcycler software. mRNA relative expression values were normalized to the housekeeping gene ABL1 Tyrosine-protein kinase1. Primers sequences used for amplification are listed in Table 5. The relative quantity of miR-223 was measured on 200 ng of total RNA by qRT-PCR using miR-223 and U6 quantitative RT-PCR were performed using the TaqMan MicroRNA specific assays (Applied Biosystem).

GENE	FORWARD	REVERSE
ABL	5'-CGCTATTCGCAATCAGGGTTA-3'	3'-GGGCGTGTGACCGTAGCT-5'
NRF2	5'-TGTAGTCTTGGTTCTAGCAGTTTC-3'	3'-TGGAACAGAGAAAGCAGAGTG-5'
HO-1	5'-CCAGCAACAAAGTGCAAGATTC-3'	3'-CCACCAGAAAGCTGAGTGTAAG-5'
G6PDH	5'-TCATCATCATGGGTGCATCGG-3'	3'-CTTGAAGAAGGGCTCACTCTGTTTG-5'
SIRT1	TaqMan assays Hs01009006_m1	
FOXO3a	5'-TCTACGAGTGGATGGTGCGTTG-3'	3'-CTCTTGCCAGTTCCCTCATTCTG-5'
SOD1	5'-CTGGACAAACCTCAGCCCTAAC-3'	3'-AACCTGAGCCTTGGACACCAAC-5'
Catalasi	5'-GTGCGGAGATTCAACACTGCCA-3'	3'-CGGCAATGTTCTCACACAGACG-5'

Table 5. Primers used

6.5 *ROS Detection*

To evaluate ROS levels cells, cells were incubated for 24 h with Zn. Mitochondrial and total ROS were assessed using the Total ROS Detection Kit (ENZ-51010, Enzo Life Sciences) and MitoSOX-based assays, following the manufacturer's instructions. Fluorescence signals were analyzed by CytoFLEX della Beckman Coulter.

6.6 Immunofluorescence

Intracellular Localization Analysis. The localization of endogenous PLZF::RARa, NRF2 and SIRT1 was assessed in cell cytospins. Briefly, cells were fixed with 4% paraformaldehyde (PFA), permeabilized, blocked, and incubated with primary antibodies. After washing, cells were incubated with Alexa Fluor 488, 555 or 647 conjugated secondary antibodies (Invitrogen, Carlsbad, CA, USA). Images were acquired using a confocal laser-scanning microscope (LSM 700, ZEISS, Jena, Germany).

6.7 *In situ proximity ligation assay (PLA)*

In situ proximity ligation assay (PLA) was performed on fixed cells using Duolin ® in Situ Orange Starter Kit (Sigma-Aldrich#DUO92102, St Louis MO, USA), according to the

manufacturer's instructions. Primary antibodies produced in rabbit (α-PLZF), in mouse (α-SIRT1) were used in combination with PLA probes (anti-rabbit PLUS and anti-mouse MINUS), each conjugated to unique DNA oligonucleotides. When target proteins interact, the DNA probes hybridize to form circular DNA, which is then amplified and detected via fluorescence. Fluorescent signals were visualized using a confocal laser scanning microscope (LSM 700, ZEISS, Jena, Germany).

6.8 Cell viability

MTS assay. Cell proliferation was assessed using the CellTiter 96® AQueous One Solution Cell Proliferation Assay (Promega, Madison, WI, USA). Cells were seeded in a 96-well plate at an initial density of 7 x 10_3 cell/well and treated for 72 h at 37 °C with the following compounds used alone or in combination: azacytidine (AZA) at concentrations ranging from 0 to 1000 mg/ml; venetoclax (VTX) at concentrations ranging from 0 to 300 nM and ascorbate at concentrations ranging from 0 to 3 mM. Subsequently, 5 µl of assay reagent was added to each well and incubated for 4 hours at room temperature. Absorbance was measured at 490 nm using a microplate reader (Thermo Scientific™ Varioskan™ Flash Multimode Reader; Waltham, MA, USA). Synergism analysis was performed using Synergy Finder tool (https://synergyfinder.fimm.fi/synergy/synfin_docs/).

6.9 $NADP^+$/NADPH Quantification

Intracellular levels of oxidized ($NADP^+$) and reduced (NADPH) forms were measured using the NADP/NADPH-Glo™ Assay (Promega, Cat. #G9081), according to the manufacturer's instructions. Cells were lysed, and aliquots of each sample were subjected to acid or base treatment to selectively degrade NADPH or $NADP^+$, respectively. After neutralization, the NADP/NADPH-Glo™ Detection Reagent was added (1:1 ratio with the sample), and

plates were incubated for 60 minutes at room temperature. Luminescence emission was recorded at approximately 560 nm using a Thermo Scientific™ Varioskan™ Flash Multimode Reader (Waltham, MA, USA). Relative luminescence units were normalized to total protein content.

6.10 *Catalase Activity Assay*

Catalase enzymatic activity was determined using the Amplex® Red Catalase Assay Kit (Invitrogen, Cat. #A22180), following the manufacturer's protocol. Briefly, cell lysates were incubated with hydrogen peroxide (H_2O_2, 40 µM final concentration) for 30 minutes at room temperature. Residual H_2O_2 was then quantified by adding the Amplex® Red reagent (50 µM) in the presence of horseradish peroxidase (HRP, 0.2 U/mL), leading to the formation of the fluorescent product resorufin. Fluorescence intensity, inversely proportional to catalase activity, was measured using a Thermo Scientific™ Varioskan™ Flash Multimode Reader (Waltham, MA, USA) with excitation at 530 and emission at 590.

6.11 *Bioenergetic analysis and characterization of primary AML blast and cell line*

Seahorse Metabolic Assays. Primary AML blast and AML cell lines were washed twice with Seahorse XF RPMI medium supplemented with 1 mM pyruvate, 2 mM glutamine, and 10 mM glucose for the XF Cell Mito Stress Test, ATP Rate Assay, and Glycolytic Rate Assay. Meanwhile, the XFe96 cartridge was loaded with drugs to reach these final concentrations:
XF Cell Mito Stress Test: oligomycin 2 µM, FCCP 1.5 µM, rotenone/antimycin A (R/A) 0.5 µM.
XF Glycolysis Stress Test: glucose 10 mM, oligomycin 2 µM, 2-deoxy-glucose (2-DG) 50 mM.
XF Real-Time ATP Rate Assay: oligomycin 2 µM, R/A 0.5 µM.
XF Glycolytic Rate Assay: R/A 0.5 µM, 2-DG 50 mM.
XF Mito Fuel Flex Test: BPTES 3 µM, etomoxir 4 µM, UK5099 2 µM.

Cells were seeded in microplates and loaded into Seahorse XFe96 Extracellular Flux Analyzer (Seahorse Bioscience- Agilent) and assays were conducted according to the manufacturer's protocols.

XF Cell Mito Stress Test assesses key parameters of mitochondrial function by directly measuring the oxygen consumption rate (OCR) of cells in basal conditions and following sequential treatment with specific inhibitors: oligomycin (to reveal respiration linked to proton leak), FCCP (to measure maximal uncoupled respiration), and Rotenone/Antimycin A (to inhibit oxidative phosphorylation and confirm that oxygen consumption is mitochondrial in origin).

XF Glycolysis Stress Test measures glycolytic function by directly quantifying the extracellular acidification rate (ECAR) of cells under basal conditions and after sequential administration of glucose (to determine basal glycolytic rate), oligomycin (to inhibit mitochondrial ATP production and reveal maximal glycolytic capacity), and 2-deoxy-D-glucose (2-DG; to inhibit glycolysis and confirm assay specificity).

XF Glycolytic Rate Assay provides precise measurements of basal glycolytic rates and compensatory glycolysis following mitochondrial inhibition. This assay accounts for CO_2 contribution to extracellular acidification from mitochondrial/TCA cycle activity, allowing direct comparison with lactate accumulation data upon treatment with rotenone/antimycin A and 2-DG.

XF Real-Time ATP Rate Assay quantifies ATP production rates from both glycolysis and mitochondrial oxidative phosphorylation simultaneously.
This is achieved by treating cells with rotenone/antimycin A (to inhibit oxidative respiration) and measuring the resulting changes in ATP production.

XF Mito Fuel Flex Test assesses mitochondrial fuel utilization in live cells by evaluating cellular dependency, capacity, and flexibility in

oxidizing three key fuels: glucose (via pyruvate), glutamine (via glutamate), and long-chain fatty acids. The oxidation rates are determined by sequential administration of pathway-specific inhibitors—UK5099 (glucose oxidation inhibitor), BPTES (glutamine oxidation inhibitor), and etomoxir (fatty acid oxidation inhibitor).

6.12 Data analysis

Data are presented as mean ± standard error of the mean (SEM). Survival analyses were performed using Kaplan–Meier estimates. Comparisons between two groups were conducted with Student's t-test, while multiple group comparisons utilized one-way or two-way ANOVA. Post-hoc analyses were performed using Bonferroni or Tukey tests, as appropriate. All statistical analyses were conducted using GraphPad Prism 5 software.

7. REFERENCES

1. Orkin, S.H. and L.I. Zon, *Hematopoiesis: an evolving paradigm for stem cell biology.* Cell, 2008. **132**(4): p. 631-44.
2. Xu, J., et al., *Crosstalk between DNA Damage Repair and Metabolic Regulation in Hematopoietic Stem Cells.* Cells, 2024. **13**(9).
3. Kohli, L. and E. Passegué, *Surviving change: the metabolic journey of hematopoietic stem cells.* Trends Cell Biol, 2014. **24**(8): p. 479-87.
4. Shevyrev, D., et al., *Hematopoietic Stem Cells and the Immune System in Development and Aging.* Int J Mol Sci, 2023. **24**(6).
5. Ho, Y.H. and S. Méndez-Ferrer, *Microenvironmental contributions to hematopoietic stem cell aging.* Haematologica, 2020. **105**(1): p. 38-46.
6. MacLean, A.L. and K.L. Rudolph, *Hematopoietic stem cell aging by the niche.* Blood, 2024. **144**(4): p. 347-348.
7. Yang, F., et al., *Unraveling Heterogeneity in the Aging Hematopoietic Stem Cell Compartment: An Insight From Single-cell Approaches.* Hemasphere, 2023. **7**(6): p. e895.
8. Cho, R.H., H.B. Sieburg, and C.E. Muller-Sieburg, *A new mechanism for the aging of hematopoietic stem cells: aging changes the clonal composition of the stem cell compartment but not individual stem cells.* Blood, 2008. **111**(12): p. 5553-61.
9. Kindler, V., et al., *Haematopoietic stem cells and mesenchymal stem cells as tools for present and future cellular therapies.* Swiss Med Wkly, 2006. **136**(21-22): p. 333-7.
10. Vardiman, J.W., et al., *The 2008 revision of the World Health Organization (WHO) classification of myeloid neoplasms and acute leukemia: rationale and important changes.* Blood, 2009. **114**(5): p. 937-51.

11. Gupta, G., et al., *Myelodysplastic syndromes/neoplasms: recent classification system based on World Health Organization Classification of Tumors - International Agency for Research on Cancer for Hematopoietic and Lymphoid Tissues.* J Blood Med, 2010. **1**: p. 171-82.
12. Amin, H.M., et al., *Having a higher blast percentage in circulation than bone marrow: clinical implications in myelodysplastic syndrome and acute lymphoid and myeloid leukemias.* Leukemia, 2005. **19**(9): p. 1567-72.
13. Döhner, H., D.J. Weisdorf, and C.D. Bloomfield, *Acute Myeloid Leukemia.* N Engl J Med, 2015. **373**(12): p. 1136-52.
14. Shipley, J.L. and J.N. Butera, *Acute myelogenous leukemia.* Exp Hematol, 2009. **37**(6): p. 649-58.
15. Shlush, L.I., *Age-related clonal hematopoiesis.* Blood, 2018. **131**(5): p. 496-504.
16. Yamamoto, J.F. and M.T. Goodman, *Patterns of leukemia incidence in the United States by subtype and demographic characteristics, 1997-2002.* Cancer Causes Control, 2008. **19**(4): p. 379-90.
17. Shah, A., et al., *Survival and cure of acute myeloid leukaemia in England, 1971-2006: a population-based study.* Br J Haematol, 2013. **162**(4): p. 509-16.
18. Zhang, J., X. Gao, and L. Yu, *Roles of Histone Deacetylases in Acute Myeloid Leukemia With Fusion Proteins.* Front Oncol, 2021. **11**: p. 741746.
19. Shimony, S., M. Stahl, and R.M. Stone, *Acute myeloid leukemia: 2023 update on diagnosis, risk-stratification, and management.* Am J Hematol, 2023. **98**(3): p. 502-526.
20. Weinberg, O.K., et al., *The International Consensus Classification of acute myeloid leukemia.* Virchows Arch, 2023. **482**(1): p. 27-37.
21. Khoury, J.D., et al., *The 5th edition of the World Health Organization Classification of Haematolymphoid Tumours:*

Myeloid and Histiocytic/Dendritic Neoplasms. Leukemia, 2022. **36**(7): p. 1703-1719.
22. Arber, D.A., et al., *The 2016 revision to the World Health Organization classification of myeloid neoplasms and acute leukemia.* Blood, 2016. **127**(20): p. 2391-405.
23. Testa, U. and F. Lo-Coco, *Targeting of leukemia-initiating cells in acute promyelocytic leukemia.* Stem Cell Investig, 2015. **2**: p. 8.
24. Hussain, L., et al., *Acute promyelocytic leukemia and variant fusion proteins: PLZF-RARα fusion protein at a glance.* Semin Oncol, 2019. **46**(2): p. 133-144.
25. Petti, M.C., et al., *Complete remission through blast cell differentiation in PLZF/RARalpha-positive acute promyelocytic leukemia: in vitro and in vivo studies.* Blood, 2002. **100**(3): p. 1065-7.
26. Lo-Coco, F., et al., *Acute promyelocytic leukemia: recent advances in diagnosis and management.* Semin Oncol, 2008. **35**(4): p. 401-9.
27. Suliman, B.A., D. Xu, and B.R. Williams, *The promyelocytic leukemia zinc finger protein: two decades of molecular oncology.* Front Oncol, 2012. **2**: p. 74.
28. Zhang, X., et al., *Current views on the genetic landscape and management of variant acute promyelocytic leukemia.* Biomark Res, 2021. **9**(1): p. 33.
29. Udensi, U.K. and P.B. Tchounwou, *Dual effect of oxidative stress on leukemia cancer induction and treatment.* J Exp Clin Cancer Res, 2014. **33**: p. 106.
30. Jansen, J.H. and B. Löwenberg, *Acute promyelocytic leukemia with a PLZF-RARalpha fusion protein.* Semin Hematol, 2001. **38**(1): p. 37-41.
31. WARBURG, O., *On the origin of cancer cells.* Science, 1956. **123**(3191): p. 309-14.
32. Desquiret, V., et al., *Dinitrophenol-induced mitochondrial uncoupling in vivo triggers respiratory adaptation in*

HepG2 cells. Biochim Biophys Acta, 2006. **1757**(1): p. 21-30.
33. Gatenby, R.A. and E.T. Gawlinski, *The glycolytic phenotype in carcinogenesis and tumor invasion: insights through mathematical models.* Cancer Res, 2003. **63**(14): p. 3847-54.
34. Yu, H. and L. Yan, *Mitochondrial metabolism: Critical mechanisms underpinning normal hematopoietic stem cell and acute myeloid leukemia stem cell function.* Gene, 2025. **966**: p. 149685.
35. Chen, W.L., et al., *A distinct glucose metabolism signature of acute myeloid leukemia with prognostic value.* Blood, 2014. **124**(10): p. 1645-54.
36. Medina, R.A. and G.I. Owen, *Glucose transporters: expression, regulation and cancer.* Biol Res, 2002. **35**(1): p. 9-26.
37. Wang, Y., et al., *Rapid diagnosis and prognosis of de novo acute myeloid leukemia by serum metabonomic analysis.* J Proteome Res, 2013. **12**(10): p. 4393-401.
38. Willems, L., et al., *Inhibiting glutamine uptake represents an attractive new strategy for treating acute myeloid leukemia.* Blood, 2013. **122**(20): p. 3521-32.
39. Catalano, G., et al., *MCL1 regulates AML cells metabolism via direct interaction with HK2. Metabolic signature at onset predicts overall survival in AMLs' patients.* Leukemia, 2023. **37**(8): p. 1600-1610.
40. Vander Heiden, M.G., L.C. Cantley, and C.B. Thompson, *Understanding the Warburg effect: the metabolic requirements of cell proliferation.* Science, 2009. **324**(5930): p. 1029-33.
41. Peng, M., et al., *Targeting Mitochondrial Oxidative Phosphorylation Eradicates Acute Myeloid Leukemic Stem Cells.* Front Oncol, 2022. **12**: p. 899502.
42. Romo-González, M., C. Ijurko, and Á. Hernández-Hernández, *Reactive Oxygen Species and Metabolism in*

Leukemia: A Dangerous Liaison. Front Immunol, 2022. **13**: p. 889875.
43. Sujobert, P. and J. Tamburini, *Co-activation of AMPK and mTORC1 as a new therapeutic option for acute myeloid leukemia.* Mol Cell Oncol, 2016. **3**(4): p. e1071303.
44. Christofk, H.R., et al., *The M2 splice isoform of pyruvate kinase is important for cancer metabolism and tumour growth.* Nature, 2008. **452**(7184): p. 230-3.
45. Fantin, V.R., J. St-Pierre, and P. Leder, *Attenuation of LDH-A expression uncovers a link between glycolysis, mitochondrial physiology, and tumor maintenance.* Cancer Cell, 2006. **9**(6): p. 425-34.
46. Shim, H., et al., *c-Myc transactivation of LDH-A: implications for tumor metabolism and growth.* Proc Natl Acad Sci U S A, 1997. **94**(13): p. 6658-63.
47. Wang, Y.H., et al., *Cell-state-specific metabolic dependency in hematopoiesis and leukemogenesis.* Cell, 2014. **158**(6): p. 1309-1323.
48. Colell, A., et al., *GAPDH and autophagy preserve survival after apoptotic cytochrome c release in the absence of caspase activation.* Cell, 2007. **129**(5): p. 983-97.
49. Zhou, F., Q. Shen, and F.X. Claret, *Novel roles of reactive oxygen species in the pathogenesis of acute myeloid leukemia.* J Leukoc Biol, 2013. **94**(3): p. 423-9.
50. Kaweme, N.M., et al., *The significant role of redox system in myeloid leukemia: from pathogenesis to therapeutic applications.* Biomark Res, 2020. **8**(1): p. 63.
51. Samimi, A., et al., *The Dual Role of ROS in Hematological Malignancies: Stem Cell Protection and Cancer Cell Metastasis.* Stem Cell Rev Rep, 2020. **16**(2): p. 262-275.
52. Jomova, K., et al., *Reactive oxygen species, toxicity, oxidative stress, and antioxidants: chronic diseases and aging.* Arch Toxicol, 2023. **97**(10): p. 2499-2574.

53. Gall Trošelj, K., et al., *Oxidative Stress and Cancer Heterogeneity Orchestrate NRF2 Roles Relevant for Therapy Response.* Molecules, 2022. **27**(5).
54. Kannan, S., et al., *Targeting the NRF2/HO-1 Antioxidant Pathway in FLT3-ITD-Positive AML Enhances Therapy Efficacy.* Antioxidants (Basel), 2022. **11**(4).
55. Zimta, A.A., et al., *The Role of Nrf2 Activity in Cancer Development and Progression.* Cancers (Basel), 2019. **11**(11).
56. Banella, C., et al., *PML/RARa Interferes with NRF2 Transcriptional Activity Increasing the Sensitivity to Ascorbate of Acute Promyelocytic Leukemia Cells.* Cancers (Basel), 2019. **12**(1).
57. Gupte, R.S., et al., *Glucose-6-phosphate dehydrogenase is a regulator of vascular smooth muscle contraction*. Antioxid Redox Signal, 2011. **14**(4): p. 543-58.
58. Ahamed, A., et al., *The Emerging Roles of the Metabolic Regulator G6PD in Human Cancers.* Int J Mol Sci, 2023. **24**(24).
59. Wu, Q.J., et al., *The sirtuin family in health and disease.* Signal Transduct Target Ther, 2022. **7**(1): p. 402.
60. Brunet, A., et al., *Stress-dependent regulation of FOXO transcription factors by the SIRT1 deacetylase.* Science, 2004. **303**(5666): p. 2011-5.
61. Mizani, S., et al., *Expression Changes of SIRT1 and FOXO3a Significantly Correlate with Oxidative Stress Resistance Genes in AML Patients.* Indian J Hematol Blood Transfus, 2023. **39**(3): p. 392-401.
62. Ruiz, M.A., et al., *Hydroxymethylcytosine and demethylation of the γ-globin gene promoter during erythroid differentiation.* Epigenetics, 2015. **10**(5): p. 397-407.
63. Travaglini, S., et al., *The Anti-Leukemia Effect of Ascorbic Acid: From the Pro-Oxidant Potential to the Epigenetic*

Role in Acute Myeloid Leukemia. Front Cell Dev Biol, 2022. **10**: p. 930205.
64. Noguera, N.I., et al., *High-dose ascorbate and arsenic trioxide selectively kill acute myeloid leukemia and acute promyelocytic leukemia blasts in vitro.* Oncotarget, 2017. **8**(20): p. 32550-32565.
65. Chen, Q., et al., *Pharmacologic doses of ascorbate act as a prooxidant and decrease growth of aggressive tumor xenografts in mice.* Proc Natl Acad Sci U S A, 2008. **105**(32): p. 11105-9.
66. Lu, J., E.H. Chew, and A. Holmgren, *Targeting thioredoxin reductase is a basis for cancer therapy by arsenic trioxide.* Proc Natl Acad Sci U S A, 2007. **104**(30): p. 12288-93.
67. DiNardo, C.D., et al., *Azacitidine and Venetoclax in Previously Untreated Acute Myeloid Leukemia.* N Engl J Med, 2020. **383**(7): p. 617-629.
68. Allis, C.D. and T. Jenuwein, *The molecular hallmarks of epigenetic control.* Nat Rev Genet, 2016. **17**(8): p. 487-500.
69. Li, Y., L. Dou, and C. Nervi, *Editorial: Genetic/epigenetic mechanisms and related clinical strategy in leukemia.* Front Oncol, 2023. **13**: p. 1275992.
70. Lu, C., et al., *IDH mutation impairs histone demethylation and results in a block to cell differentiation.* Nature, 2012. **483**(7390): p. 474-8.
71. Xie, N., et al., *NAD.* Signal Transduct Target Ther, 2020. **5**(1): p. 227.
72. Grignani, F., et al., *Fusion proteins of the retinoic acid receptor-alpha recruit histone deacetylase in promyelocytic leukaemia.* Nature, 1998. **391**(6669): p. 815-8.
73. Martín, I., et al., *Synergistic Antioncogenic Activity of Azacitidine and Curcumin in Myeloid Leukemia Cell Lines and Patient Samples.* Anticancer Res, 2019. **39**(9): p. 4757-4766.
74. Gemuenden, C., et al., *Efficacy of Azacitidine in De Novo and Relapsed Acute Myeloid Leukemia: A Retrospective*

Comparative Study. Clin Lymphoma Myeloma Leuk, 2015. **15**(12): p. 811-5.
75. Nervi, C., F. Fazi, and F. Grignani, *Oncoproteins, heterochromatin silencing and microRNAs: a new link for leukemogenesis.* Epigenetics, 2008. **3**(1): p. 1-4.
76. Zardo, G., et al., *Polycombs and microRNA-223 regulate human granulopoiesis by transcriptional control of target gene expression.* Blood, 2012. **119**(17): p. 4034-46.
77. Billi, M., et al., *Nuclear miRNAs: Gene Regulation Activities.* Int J Mol Sci, 2024. **25**(11).
78. Marson, A., et al., *Connecting microRNA genes to the core transcriptional regulatory circuitry of embryonic stem cells.* Cell, 2008. **134**(3): p. 521-33.
79. Anelli, L., et al., *Dysregulation of miRNA in Leukemia: Exploiting miRNA Expression Profiles as Biomarkers.* Int J Mol Sci, 2021. **22**(13).
80. Issah, M.A., et al., *Epigenetic modifications in acute myeloid leukemia: The emerging role of circular RNAs (Review).* Int J Oncol, 2021. **59**(6).
81. Panina, S.B., J. Pei, and N.V. Kirienko, *Mitochondrial metabolism as a target for acute myeloid leukemia treatment.* Cancer Metab, 2021. **9**(1): p. 17.
82. Ding, N., et al., *Dynamic and Static Regulation of Nicotinamide Adenine Dinucleotide Phosphate: Strategies, Challenges, and Future Directions in Metabolic Engineering.* Molecules, 2024. **29**(15).
83. Hashemi, M., et al., *SIRT1 as a masterful reciprocal regulator of molecular mechanisms and signaling pathways involved in tumor growth and expansion.* Clin Exp Med, 2025. **25**(1): p. 225.
84. Zhou, Z., et al., *Successfully treatment of PLZF-RARα positive acute promyelocytic leukemia by Venetoclax combining with decitabine: a case report and literature review.* Hematology, 2024. **29**(1): p. 2399362.

85. Cicconi, L. and F. Lo-Coco, *Current management of newly diagnosed acute promyelocytic leukemia.* Ann Oncol, 2016. **27**(8): p. 1474-81.
86. Zaza, A., et al., *PML::RARα+ myeloid cells display metabolic alterations that can be targeted to treat resistant/relapse acute promyelocytic leukemias.* Leukemia, 2025.
87. Olmos, Y., et al., *SirT1 regulation of antioxidant genes is dependent on the formation of a FoxO3a/PGC-1α complex.* Antioxid Redox Signal, 2013. **19**(13): p. 1507-21.

Ringraziamenti

Al termine di questo percorso di dottorato desidero esprimere la mia sincera gratitudine alla Prof.ssa Nelida Noguera e al Prof. Gianfranco Catalano, per avermi seguita con costanza, attenzione e grande disponibilità. Un ringraziamento particolarmente affettuoso va alla Prof.ssa Nelida Noguera, tutor esterna del PhD, per la fiducia che ha riposto in me e per avermi guidata con passione e dedizione, trasmettendomi l'importanza della perseveranza, della determinazione e del rigore nel lavoro scientifico.

Un sentito ringraziamento va ai membri del laboratorio della Prof.ssa Nelida Noguera, alla Dott.ssa Gloria Pasqualini e al Dott. Eliezer Barroso, per il supporto scientifico, la disponibilità e la collaborazione che hanno reso il lavoro quotidiano stimolante e formativo.

Desidero inoltre ringraziare la Prof.ssa Clara Nervi, tutor interno della mia tesi, per il supporto, la disponibilità e la precisione dimostrati nel corso di questo lavoro, nonché per le indicazioni e le correzioni puntuali e preziose che hanno contribuito in modo determinante alla realizzazione della tesi.

Ringrazio anche tutti i membri del laboratorio della Prof.ssa Clara Nervi, la Dott.ssa Elisabetta De Marini e la Dott.ssa Martina Gentile per il confronto scientifico e il contributo offerto durante lo svolgimento del lavoro sperimentale.

Un ringraziamento speciale va alla mia famiglia, ai miei genitori Antonella e Michele e a mio fratello Federico, per essermi stati sempre vicini e per avermi sostenuta lungo questi anni di studio. Li ringrazio per i preziosi consigli, per l'ascolto e per la comprensione che non mi hanno mai fatto mancare.

Desidero ringraziare i miei amici per essermi stati sempre vicini, per il sostegno e l'incoraggiamento durante questo percorso:
A Barbara, Eugenia, Michele e il gruppo di Statte, ai miei amici di Taranto e agli amici The Camillos.

Ringrazio i colleghi dei laboratori del terzo piano, che nel tempo sono diventati molto più che semplici colleghi. Lucia, Daniel, Francesca C, Giulia, Olga, la mia compagna di stanza cellule Francesca M e Camilla.

Infine, ringrazio Pierangelo, il mio fidanzato, per essere stato al mio fianco nell'ultima fase di questo percorso.